GAUSSIAN FILTERED REPRESENTATIONS OF IMAGES

Gaussian filtered representations of images have been used to address several important visual tasks. In early work Marr and Hildreth used them to attenuate noise and detect edges (1). Specific operators such as the Laplacian of Gaussians and the difference of Gaussians have been used for multiresolution analysis of images (2,3). More recently, several researchers (4,5,6,7,8) have shown that Gaussian derivatives may be used to robustly represent the local image structure at multiple scales. In this article, the Gaussian derivative filter and its spatial- and frequency-domain properties are examined, and it is used to create a description of the local intensity surface. Motivated by its multiscale properties, Gaussian filtered representations are constructed to address two specific problems.

The first problem considered is of matching images that are affine deformed versions of each other. Solutions to this problem form an important component for several applications such as video mosaicking, registration, object recognition, structure from motion, and shape from texture. In particular, consider an example where successive views of a scene are observed in a video. These views will be deformed versions of each other and under certain circumstances may be approximated using an affine transformation. Gaussians and their derivatives are used to recover affine deformations. Consider two patches related by an affine transform. If the patches are filtered using Gaussian filters, the outputs are equal provided the Gaussian is affine-transformed in the same manner as the function. Thus, one can construct a solution that minimizes the error with respect to the affine parameters, where the error is defined between corresponding Gaussian derivative filter outputs. The affine matching problem is discussed in detail in the section after next.

The second focus of this article is in addressing the problem of image retrieval. Advances in computational power and the rapid increase in performance-to-cost ratio of most computational devices has led to the acquisition and storage of pictorial information on digital media. One of the important challenges that this trend presents is the development of algorithms for managing digitally stored pictorial information. While machine-stored text can be searched using any of several text search engines, there are as yet no good tools available to search and manage image collections.

The reason that *image retrieval* has proven to be hard is that users expect the system to find relevant images based on some personal or cultural semantics. Representing semantics is hard and requires solutions to problem such as automatic feature detection, segmentation, and recognition. These problems are as yet unsolved. However, in certain cases, many image attributes such as color, texture, shape, and "appearance" are often directly correlated with the semantics of the problem. For example, logos or product packages (e.g., a box of Tide) have the same color wherever they are found. The coat of a leopard has a unique texture, and Abraham Lincoln's appearance is distinctive. These image attributes can often be used to index and retrieve images.

One such approach is to exploit the structure of the image intensity surface. In recent work Ravela and Manmatha (9) have shown that representations of the intensity surface may be used to retrieve objects that appear visually similar. Arguably an object's visual appearance in an image is closely related to several factors, including, among others, its three-dimensional shape, albedo, and surface texture and the image viewpoint. It is nontrivial to separate the different factors constituting an object's appearance. For example, the face of a person has a unique appearance that cannot just be characterized by the geometric shape of the "component parts."

We argue that Gaussian filtered representation of images can be used for retrieval by appearance. A paradigm for retrieval that is used widely, and is adopted here, is that images in the database are processed and described by a set of feature vectors. These vectors are indexed ahead of time. During run time, a query is provided in the form of an example image, and its features are compared with those stored. Images are then retrieved in the order indicated by the comparison operator. In this work, feature vectors are constructed using responses to Gaussian derivatives filters at multiple scales. Using this approach, it is shown that whole images or parts thereof can be retrieved. This flexibility is important because a user interacting with an image retrieval system might be interested in the image as a whole, such as a trademark, or in only a part of the image, such as a face within a scene. In the former case the representation must capture the appearance of the whole image, and the similarity is global. In the latter case, the representation must allow for local similarity.

The remainder of this article is organized as follows. The next section provides a review of the Gaussian filter, some key properties and derives the features that will be used subsequently to address the affine image matching and retrieval tasks. In the subsequent section matching of images under an affine deformation is considered, and in the last section image retrieval by appearance is discussed.

THE GAUSSIAN FILTERED REPRESENTATION OF IMAGES

This section begins by examining the spatial and frequency characteristics of the Gaussian filter. Then, the role of the Gaussian filter in providing a robust representation of the intensity surface is discussed. The section ends with a discussion of how to implement discrete versions of Gaussians and their derivatives.

The Gaussian Filter: Preliminaries

The Gaussian and Its Derivatives. The isotropic normalized Gaussian in two dimensions is a C^∞ smooth function, defined as

$$G(\boldsymbol{p}, \sigma) = \frac{1}{2\pi\sigma^2} e^{-\boldsymbol{p}^{\mathrm{T}}\boldsymbol{p}/2\sigma^2} \tag{1}$$

where $\boldsymbol{p} = \langle x, y\rangle \in R^2$, and $\sigma \in R$ is referred to as the scale. The derivatives of the normalized Gaussian are defined to arbitrary order. The nth derivative of the Gaussian (in two dimensions) is written in tensor form as

$$G_{i_1 \ldots i_n}(\cdot, \sigma) = \frac{\delta^n G(\cdot, \sigma)}{\delta i_1 \cdots \delta i_n} \tag{2}$$

where the free variables $i_1, \ldots, i_n$ cycle through all the degrees of freedom (x, y). Thus the first derivative is written as G_{i_1}, which in the Cartesian frame is G_x and G_y.

Filtering. In the spatial domain, the discrete two-dimensional (2D) image $Z(\boldsymbol{p})$ filtered with the Gaussian is expressed as the discrete convolution, $I(\boldsymbol{p}, \sigma) = (Z \star G)(\boldsymbol{p}, \sigma)$ the Gaussian has infinite extent. Since discrete images are typically of finite extent, the truncation of the Gaussian extent is considered the subsection "Implementation." In the case of Gaussian derivatives, since differentiation commutes with convolution, the following expression may be written:

$$\begin{aligned} I_{i_1 \ldots i_n}(\boldsymbol{x}, \sigma) &= (Z \star G)_{i_1 \ldots i_n}(\boldsymbol{x}, \sigma) \\ &= (Z_{i_1 \ldots i_n} \star G)(\boldsymbol{x}, \sigma) = (Z \star G_{i_1 \ldots i_n})(\boldsymbol{x}, \sigma) \end{aligned} \tag{3}$$

Frequency-Domain Interpretation. The Fourier transform of the 2-D Gaussian defined in Eq. (1) is written as

$$\mathscr{G}(\boldsymbol{u}, \sigma) = e^{-\sigma^2 \boldsymbol{u}^{\mathrm{T}}\boldsymbol{u}/2} \tag{4}$$

where $\boldsymbol{u} = \langle u_x, u_y\rangle \in R^2$ is the 2D frequency variable. Similarly, the Fourier transform of the nth derivative of the Gaussian defined in Eq. (2) is defined as

$$\mathscr{G}^{(i_1 \ldots i_n)}(\boldsymbol{u}, \sigma) = j^n (u_{i_1} \ldots u_{i_n}) \mathscr{G}(\boldsymbol{u}, \sigma) \tag{5}$$

Here, $i_1, \ldots, i_n$ are free variables that can be identified with any of the Cartesian degrees of freedom, and $j = \sqrt{-1}$. For example, the Fourier transform of the second mixed derivative G_{xy} is $\mathscr{G}^{(i_1 i_2)}(u, \sigma) = -u_x u_y \mathscr{G}(\boldsymbol{u}, \sigma)$, where the substitution $i_1 = x$ and $i_2 = y$ is made. In a Cartesian coordinate system the Fourier transform of the nth Gaussian derivative may be written as

$$\mathscr{G}^{(i_1 \ldots i_n)}(\boldsymbol{u}, \sigma) = \mathscr{G}^{(x^p y^q)}(\boldsymbol{u}, \sigma) = j^{p+q}(u_z^p u_y^q)\mathscr{G}(\boldsymbol{u}, \sigma) \tag{6}$$

for some integers $p, q \geq 0$, $p + q = n$, and then p free variables are instantiated to x and q to y.

From the above two definitions, using composition, one may immediately observe the following properties:

Cartesian Separability. The Fourier transform of the nth Gaussian derivative may be expressed as the composition of one-dimensional (1-D) filters:

$$\begin{aligned} j^{p+q}(u_x^p u_y^q)\mathscr{G}(\boldsymbol{u},\sigma) &= j^p u_x^p e^{-\sigma^2 u_x^2/2} \cdot j^q u_x^q e^{-\sigma^2 u_y^2/2} \\ &= \mathscr{H}_x^{(p)}(u_x,\sigma)\cdot \mathscr{H}_y^{(q)}(u_y,\sigma) \end{aligned} \tag{7}$$

Since composition implies convolution in the spatial domain, one can implement the nth Gaussian derivative using separable 1-D convolutions.

Cascade Property. The cascade property of Gaussian derivatives may be observed from the composition of two filters in the frequency domain:

$$\mathscr{G}^{(x^p y^q)}(\boldsymbol{u},\sigma_1)\cdot \mathscr{G}^{(x^m y^n)}(\boldsymbol{u},\sigma_2) = \mathscr{G}^{(x^{p+m} y^{q+n})}(\boldsymbol{u},\sqrt{\sigma_1^2+\sigma_2^2}) \tag{8}$$

Thus, filtering a signal successively with several Gaussian filters of scales $\sigma_1, \ldots, \sigma_n$ is equivalent to filtering the signal with a single Gaussian filter of scale $\sigma = \sqrt{\sigma_1^2 + \cdots + \sigma_n^2}$.

Center Frequency and Bandwidth. The Gaussian filter is a low-pass filter, and the derivatives are bandpass filters. In what follows, the center frequency and bandwidth of the nth derivative of the (spatial) Gaussian are derived. For the sake of simplicity 1-D Gaussians are considered.

The Fourier transform of the nth derivative of a 1D Gaussian G_{x^n} is written as

$$\mathscr{G}^{(x^n)}(u,\sigma) = j^n u^n e^{-\sigma^2 u^2/2}$$

Differentiating with respect to u and computing the extremum, one obtains the center frequency u_0:

$$\begin{aligned} \frac{d\mathscr{G}^{(x^n)}(u,\sigma)}{du} &= (n - u^2\sigma^2) j^n u^{n-1} e^{-\sigma^2 u^2/2} = 0 \\ u_0 &= \pm\frac{\sqrt{n}}{\sigma} \end{aligned} \tag{9}$$

It should be noted that the 1D function $\mathscr{G}^{(x^n)}$ is unimodal in either half plane and has a Gaussian envelope. It is odd and imaginary for odd-order spatial derivatives, and even and real for even-order spatial derivatives. This equation states that the center frequency is coupled both to the bandwidth and to the order of the derivative. As the order of the derivative increases, so does its center frequency, and therefore, higher derivatives enhance higher levels of spatial detail.

There are several ways to define the bandwidth of the filter. Here we adopt the equivalent-rectangular-bandwidth formulation (10). This formulation equates the area under the power spectrum of the filter with that of an equivalent ideal filter of width W and height equal to the peak instantaneous power of the filter. Therefore, one may write

$$W \times |(ju_0)^n e^{-\sigma^2 u_0^2/2}|^2 = \int_0^\infty |(ju)^n e^{-\sigma^2 u^2/2}|^2\, du \tag{10}$$

After some manipulation the solution to this relation can be shown to be the following:

$$W = W(n,\sigma) = \frac{e^n \pi}{4\sigma n^n}\prod_{i=1}^{i=n}(i - \tfrac{1}{2}), \qquad n \geq 1 \tag{11}$$

$$W(0,\sigma) = \frac{\sqrt{\pi}}{\sigma} \tag{12}$$

The above expressions show that the center frequency and bandwidth of the Gaussian and its derivatives are related to the order and scale of the derivative in the spatial domain. The Gaussian is a low-pass filter, filter while its derivatives are band-pass filters.

Noise Attenuation. Since the Gaussian derivatives are band-pass filters, they may be used to attenuate noise. In particular, consider a 1D function $Z(x) = P(x) + \epsilon \sin(\omega_1 x)$. The Fourier transform of $z(x)$ is

$$\mathscr{Z}(u) = \mathscr{P}(u) + N(u)$$

where

$$N(u) = j\pi[\delta(u + w_1) - \delta(u - w_1)]$$

Consider the application of the nth derivative of a 1D Gaussian to $Z(x)$ using the right-hand side (RHS) of Eq. (3), that is, $I_n(x,\sigma) = Z(x) \bigstar G_n(x,\sigma)$. The Fourier transform of $I_n(x,\sigma)$ is

$$\begin{aligned} \mathscr{I}^{(n)}(u,\sigma) &= \mathscr{G}^{(n)}(u,\sigma)\mathscr{P}(u) + \mathscr{G}^{(n)}(u,\sigma)N(u) \\ &= \cdots + j^n u^n e^{-\sigma^2 u^2/2} N(u) \end{aligned} \tag{13}$$

where $\mathscr{G}^{(n)}$ is the Fourier transform of the nth Gaussian derivative. The second term on the RHS of Eq. (13) can be made arbitrarily small by choosing an appropriate σ, eliminating the noise in the function Z. However, this also implies that the signal $\mathscr{P}(u)$ will be band-limited. Higher frequencies will get attenuated.

Representation of the Intensity Surface

The local spatial structure of the intensity surface can be approximated using the local spatial derivatives of the surface. This can be seen from the Taylor series expansion of the intensity surface. The Taylor expansion in the neighborhood of a point in the image will fully describe the local intensity surface up to the order to which the series is constructed. Consider an image I at point $\boldsymbol{p} = \langle x, y\rangle$. The value at a location $\boldsymbol{p} + \Delta\boldsymbol{p}$ can be estimated using the Taylor series expansion (written in tensor form):

$$I(\boldsymbol{p} + \Delta\boldsymbol{p}) \approx \sum_{n=0}^{N}\frac{1}{n!}\left(\Delta\boldsymbol{p}_{i_1}\cdots\Delta\boldsymbol{p}_{i_n}\frac{\delta^n I(\boldsymbol{p})}{\delta i_1\cdots\delta i_n}\right)$$

Each term i_j ($j = 1, \ldots, n$) is substituted for all the degrees of freedom, which in the case of a 2D image is two. Up to order two, the expansion becomes

$$\begin{aligned} I(\boldsymbol{p}+\Delta\boldsymbol{p}) &= \sum_{n=0}^{2}\frac{1}{n!}\left(\Delta\boldsymbol{p}_{i_1}\cdots\Delta\boldsymbol{p}_{i_n}\frac{\delta^n I(\boldsymbol{p})}{\delta i_1\cdots\delta i_n}\right) \\ &= I(\boldsymbol{p}) + \Delta\boldsymbol{p}_{i_1}\frac{\partial I(\boldsymbol{p})}{\partial i_1} + \frac{1}{2!}\left(\Delta\boldsymbol{p}_{i_1}\Delta\boldsymbol{p}_{i_2}\frac{\delta^2 I(\boldsymbol{p})}{\delta i_1\delta i_2}\right) \\ &= I(\boldsymbol{p}) + \Delta\boldsymbol{p}_x\frac{\delta I(\boldsymbol{p})}{\delta x} \\ &\quad + \frac{1}{2!}\left(\Delta\boldsymbol{p}_x^2\frac{\delta^2 I(\boldsymbol{p})}{\delta x^2} + \Delta\boldsymbol{p}_x\,\Delta\boldsymbol{p}_y\frac{\delta^2 I(\boldsymbol{p})}{\delta x\delta y}\right) \\ &\quad + \Delta\boldsymbol{p}_y\frac{\delta I(\boldsymbol{p})}{\delta h} + \frac{1}{2!}\left(\Delta\boldsymbol{p}_y\,\Delta\boldsymbol{p}_x\frac{\delta^2 I(\boldsymbol{p})}{\delta y\delta x} + \Delta\boldsymbol{p}_y^2\frac{\delta^2 I(\boldsymbol{p})}{\delta y^2}\right) \end{aligned}$$

Rearranging the terms, we get the more familiar Cartesian form of the Taylor series (again up to order two):

$$\begin{aligned} I(\boldsymbol{p}+\Delta\boldsymbol{p}) = I(\boldsymbol{p}) &+ \Delta\boldsymbol{p}_x\frac{\partial I(\boldsymbol{p})}{\delta x} + \Delta\boldsymbol{p}_y\frac{\partial I(\boldsymbol{p})}{\delta y} \\ &+ \frac{1}{2!}\left(\Delta\boldsymbol{p}_x^2\frac{\delta^2 I(\boldsymbol{p})}{\delta x^2} + 2\,\Delta\boldsymbol{p}_x\,\Delta\boldsymbol{p}_y\frac{\delta^2 I(\boldsymbol{p})}{\delta x\,\delta y}\right. \\ &\left. + \Delta\boldsymbol{p}_y^2\frac{\delta^2 I(\boldsymbol{p})}{\delta y^2}\right) \end{aligned}$$

The above equation states that in order to estimate the intensity in the neighborhood of a point $\boldsymbol{p}$ the derivatives at $\boldsymbol{p}$ must be known. Therefore, it can be argued that spatial derivatives may be used to approximate the local intensity surface.

In the case of digital images, which are 2-D discrete functions of finite range, derivatives may be approximated using finite-difference operators. However, while finite differences can be computed, their outputs must be meaningful, or *well conditioned,* in the presence of noise. In the preceeding subsection it is shown that adding a high-frequency, low-amplitude noise may make the derivatives unstable. In discrete images this will result in noisy measurements.

A solution to the problem lies in the fact that the derivatives of a possibly discontinuous function become well conditioned if it is first convolved with the derivative of a smooth (C^∞) test function (8). The Gaussian is a smooth test function, and therefore the derivatives of the smoothed image $I(\boldsymbol{x}, \sigma) = (Z \bigstar G)(\boldsymbol{x}, \sigma)$, $\boldsymbol{x} \in R^2$, are well conditioned for some value of σ. Another way of observing this is from the noise attenuation property presented in the preceding subsection.

The operational scheme for computing local structure at a given scale of observation σ is as follows. Each image is filtered with Gaussian derivatives (at a certain scale) to the order to which the local structure is desired to be approximated. Therefore, each pixel is associated with a set of derivatives that completely define the Taylor expansion to the desired order. Koenderink and van Doorn (5) have advocated the use of this representation and call it the local N-jet. The local N-jet of $I(\boldsymbol{x})$ at scale σ and order N is defined as the set

$$J^N[I](\boldsymbol{x},\sigma) = \{I_{i_1\ldots i_n,\sigma} | n = 0,\ldots,N\} \qquad (14)$$

Observe that $\lim_{N\to\infty} J^N[I](\boldsymbol{x}, \sigma)$ bundles all the derivatives required to fully reconstruct the surface I_σ in a locality around $\boldsymbol{x}$ at a particular scale. This is the primary observation that is used to characterize local structure. That is, up to any order the derivatives locally approximate the regularized intensity surface. As a practical example consider the local 2-jet of an image $I(\boldsymbol{p})$, $\boldsymbol{p} = \langle x, y\rangle \in R^2$, at scale σ ($I_{yx} = I_{xy}$ and is therefore dropped):

$$J^2[I](\boldsymbol{p},\sigma) = \{I, I_x, I_y, I_{xx}, I_{xy}, I_{yy}\}(\boldsymbol{p},\sigma)$$

The image I is filtered with the first two Gaussian derivatives (and the Gaussian itself) in both x and y directions. Point $\boldsymbol{p}$ is therefore associated with a *derivative feature vector* of responses at scale σ.

Multiscale Representation and Scale Space. The derivative feature vector is computed at a single scale, and therefore constitutes observations of the intensity surface at a fixed bandwidth. Equivalently, in the spatial domain, the intensity surface is observed at a fixed window size. In effect, the derivative feature vector constitutes observations, not of the original image, but of a smoothed version of it. Therefore, computing derivatives at a single scale is not likely to be a robust representation of local structure. Fundamentally, this is because the local structure of the image depends on the scale at which it is observed. An image will appear different at different scales. For example, at a small scale the texture of an ape's coat will be visible. At a large enough scale, the coat will appear homogeneous.

A better characterization of local structure is obtained by computing derivatives at several scales of observation. In the frequency domain this amounts to sampling the frequency spectrum of the original image using several bandwidths (scales) around multiple center frequencies (derivatives). In the spatial domain, it may be viewed as computing local derivatives at several neighborhoods around a point.

The Gaussian forms a very attractive choice for a multiscale operator, for several reasons. First, it is naturally defined with respect to a continuous scale parameter. Second, under certain conditions (4) it uniquely generates the linear scale space of an image.

The term *scale space* was introduced by Witkin (11) to describe the evolution of image structure over multiple scales. Starting from an original image, successively smoothed images are generated along a scale dimension. In this regard several researchers (4,6–8) have shown that the Gaussian uniquely generates the linear scale space of the image when it is required that structures present at a coarser scale must already be present at a finer scale. That is, no new structures must be introduced by the operator used to generate the scale space. Typically, these structures are the zero crossings or local maxima of the image intensity. This is a very significant result, because it provides a formal mechanism to represent multiscale information using a well-defined operator.

More formally, the scale space of an image $Z(\boldsymbol{p})$, $\boldsymbol{p} = \langle x, y\rangle \in R^2$, may be written as the one-parameter family of derived images obtained using the Gaussian operator G:

$$I(\boldsymbol{p},\sigma) = Z(\boldsymbol{p}) \star G(\boldsymbol{p},\sigma)$$

The linear scale-space representation models an important physical observation. As an object moves away from a camera (in depth), its image appears less structured and finer contrasts get blurred. The change in intensity in a locality around a pixel that occurs with changing distance is accurately represented in the scale-space trajectory of that pixel. A detailed analysis deriving the Gaussian as the unique linear scale-space operator is beyond the scope of this article. For an in-depth study the reader is pointed to Florack's dissertation (8).

From a practical perspective, the Gaussian allows local structure to be computed at several scales of observation that are related in a precise manner. Local structure as represented by the spatial derivatives may be computed directly across scales without explicitly computing the scale space. This may be seen from Eq. (3). In fact, Lindeberg (6) shows that the scale space is well defined for the Gaussian derivatives as well. Therefore, the Gaussian filtered representation is useful in at least two ways. First, it allows for the stable and efficient computation of local structure. Second, it is the only way to generate the linear scale space.

An argument is therefore made for a *multiscale feature vector* that describes the intensity surface locally at several scales. From an implementation standpoint a multiscale feature vector at a point p in an image I is simply the vector

$$J^N_{(\sigma_1\ldots\sigma_k)}[I] = \{J^N[I](\boldsymbol{p},\sigma_1), J^N[I](\boldsymbol{p},\sigma_2),\ldots,J^N[I](\boldsymbol{p},\sigma_k)\} \tag{15}$$

for some order N and a set of scales $\sigma_1, \ldots, \sigma_k$.

A natural question that arises in building representations for various applications is the parametrization required for the multiscale feature vector—that is, the number of scales to be used, their spacing, and the number of orders to be considered. In the applications described in this paper, the scales are placed half an octave ($\sqrt{2}$) apart and typically three to five scales are used. In all cases, only the first two orders are used and higher orders are ignored.

Behavior Under Coordinate Deformations

There are several additional properties that make the Gaussian a suitable operator for analysis of images. In this section we examine the behavior of the Gaussian and its derivatives with respect to coordinate deformations of the image. In particular, behavior with respect to size changes and 2-D rotations of the coordinate frame are considered.

Scaling Theorems. Gaussian derivatives may be used to compare image patches that are scaled versions of each other in a straightforward manner. Consider two images I_0 and I_1 that are scaled versions of each other (but otherwise identical). Assume that the scaling is centered at the origin. That is, $I_0(\boldsymbol{p}) = I_1(s\boldsymbol{p})$ Then the following relations hold (12,13):

$$\begin{aligned} I_0(\boldsymbol{p}) \star G(\cdot,\sigma) &= I_1(s\boldsymbol{p}) \star G(\cdot, s\sigma) \\ I_0(\boldsymbol{p}) \star G^{(k)}(\cdot,\sigma) &= I_1(s\boldsymbol{p}) \star G^{(k)}(\cdot, s\sigma) \end{aligned} \tag{16}$$

where

$$G^{(k)}(\cdot,t) = t^k G_{i_1\ldots i_k}(\cdot,t)$$

We call these the *scale-shifting theorems* or simply *scaling theorems.* These equations state that if the image I_s is a scaled version of I_0 by a factor s, then in order to compare any two corresponding points in these images the filters must also be stretched (i.e. scaled) by the same factor. For example, if a point p_0 is being compared with a point p_1 in images I_0 and I_1, where I_1 is twice the size of I_0, then for the responses to be equal, the filter used to compute the response at p_1 must be at twice the scale of that applied at p_0. This property has been exploited for matching affine deformed images (see the next section), object recognition, (14) and image retrieval (15).

Steerability. The Gaussian derivatives may be combined under rotations to synthesize filters in an arbitrary orientation. This has been called the steering property (16). This property is interesting for two reasons. First, images may be filtered using Gaussian derivatives tuned to any arbitrary orientation without actually rotating the filters. The tuned filters may be expressed as a combination of filters in a normal coordinate frame. Therefore, responses to any steered direction may be computed as a simple rotation of the responses. Thus, separable implementations are feasible even for rotated filters. Second, it may be used as a basis for generating feature vectors that are invariant to 2-D rotations as discussed in the next section. The results for the first two orders are now derived.

Consider a 2-D rotated version of the Cartesian coordinate frame $\boldsymbol{p} = \langle x, y\rangle$ written as $\boldsymbol{q} = \langle x_2, y_2\rangle$ such that $\boldsymbol{q} = \boldsymbol{R}^{\mathrm{T}}\boldsymbol{p}$, where $\boldsymbol{p}$ and $\boldsymbol{q}$ are the respective coordinates and $\boldsymbol{R}$ is the rotation matrix. Assume for simplicity that all coordinates are right handed.

Isotropy. It is straightforward to show that $G(\boldsymbol{q}, \sigma) = G(\boldsymbol{R}^{\mathrm{T}}\boldsymbol{p}, \sigma) = G(\boldsymbol{p}, \sigma)$. That is, the Gaussian is isotropic.

First Derivatives. Consider the first derivatives of the 2-D Gaussian. The following relationship holds from the circular symmetry of the Gaussian.

$$\begin{aligned} \begin{bmatrix} G_{x_2}(\boldsymbol{q},\sigma) \\ G_{y_2}(\boldsymbol{q},\sigma) \end{bmatrix} &= -\frac{1}{\sigma^2}\boldsymbol{q}G(\boldsymbol{q},\sigma) \\ &= -\frac{1}{\sigma^2}(\boldsymbol{R}^{\mathrm{T}}\boldsymbol{p})G(\boldsymbol{R}^{\mathrm{T}}\boldsymbol{p},\sigma) \\ &= \boldsymbol{R}^{\mathrm{T}}\left(-\frac{1}{\sigma^2}(\boldsymbol{p})G(\boldsymbol{p},\sigma)\right) \\ &= \boldsymbol{R}^{\mathrm{T}}\begin{bmatrix} G_x(\boldsymbol{p},\sigma) \\ G_y(\boldsymbol{p},\sigma) \end{bmatrix} \end{aligned} \tag{17}$$

Second Derivatives. Similarly, the second derivative may also be steered:

$$\begin{aligned} &\begin{bmatrix} G_{x_2y_2}(\boldsymbol{q},\sigma) & G_{x_2y_2}(\boldsymbol{q},\sigma) \\ G_{y_2x_2}(\boldsymbol{q},\sigma) & G_{y_2y_2}(\boldsymbol{q},\sigma) \end{bmatrix} \\ &= \frac{1}{\sigma^2}\left(\frac{1}{\sigma^2}\begin{bmatrix} x_2^2 & x_2y_2 \\ x_2y_2 & y_2^2 \end{bmatrix} - \boldsymbol{I}_2\right) G(\boldsymbol{q},\sigma) \\ &= \frac{1}{\sigma^2}\left(\frac{1}{\sigma^2}\boldsymbol{q}\boldsymbol{q}^{\mathrm{T}} - \boldsymbol{I}_2\right) G(\boldsymbol{q},\sigma) \\ &= \frac{1}{\sigma^2}\left(\frac{1}{\sigma^2}\boldsymbol{R}^{\mathrm{T}}\boldsymbol{p}\boldsymbol{p}^{\mathrm{T}}\boldsymbol{R} - \boldsymbol{I}_2\right) G(\boldsymbol{R}\boldsymbol{p},\sigma) \\ &= \boldsymbol{R}^{\mathrm{T}}\frac{1}{\sigma^2}\left(\frac{1}{\sigma^2}\boldsymbol{p}\boldsymbol{p}^{\mathrm{T}} - \boldsymbol{I}_2\right) G(\boldsymbol{p},\sigma)\boldsymbol{R} \\ &= \boldsymbol{R}^{\mathrm{T}}\begin{bmatrix} G_{xx}(\boldsymbol{p},\sigma) & G_{xy}(\boldsymbol{p},\sigma) \\ G_{yz}(\boldsymbol{p},\sigma) & G_{yy}(\boldsymbol{p},\sigma) \end{bmatrix}\boldsymbol{R} \end{aligned} \tag{18}$$

where

$$\boldsymbol{I}_2 = \begin{bmatrix} 1 & 0 \\ 0 & 1 \end{bmatrix}$$

Several authors have exploited the steerability property of Gaussian derivatives.

Rao and Ballard (14) steered multiscale derivative vectors so as to represent the orientation with the best local responses, and Ravela et al. (17) exploited steerability to track image patches. In the next section this property is used in conjunction with differential invariants to construct multiscale invariant vectors that are derivatives expressed in the local coordinate frame and are invariant to 2-D rotations.

Rotational Invariants. Gaussian derivatives may be steered to any given orientation. Therefore, the image derivatives can be stably computed along any orientation using Gaussian derivatives tuned to that orientation. This property allows the creation of *features* that are invariant to 2-D rotations of the image plane.

It is well known (6) that if some property of the local intensity surface is used to define a local coordinate frame that is a rotation of the image coordinate frame, then derivatives computed in the local frame will be invariant to rotations of the intensity surface. For example, assume that a new coordinate frame is defined by the local gradient direction in the image I. In the above-mentioned framework let the axis y_2 represent a direction parallel to the local gradient, and let x_2 be orthogonal to it in a right-hand coordinate sense. Then one may define an orthonormal matrix $\boldsymbol{R}$ such that

$$\boldsymbol{R} = \frac{1}{\sqrt{I_x^2 + I_y^2}} \begin{bmatrix} I_y & I_x \\ -I_x & I_y \end{bmatrix} \tag{19}$$

Note that the matrix $\boldsymbol{R}$ is defined locally at every point. The new coordinate frame $\langle x_2, y_2 \rangle$ will likely change from pixel to pixel, but is automatically determined. Thus, an image filtered with the first Gaussian derivative steered to the $\langle x_2, y_2 \rangle$ coordinate frame can be equivalently expressed in the image coordinate frame $\langle x, y \rangle$ in the following manner:

$$\begin{aligned} \begin{bmatrix} I_{x_2} \\ I_{y_2} \end{bmatrix} &= Z \star \begin{bmatrix} G_{x_2} \\ G_{y_2} \end{bmatrix} = Z \star \boldsymbol{R}^{\mathrm{T}} \begin{bmatrix} G_x \\ G_y \end{bmatrix} \\ &= \boldsymbol{R}^{\mathrm{T}} \begin{bmatrix} Z \star G_x \\ Z \star G_y \end{bmatrix} = \begin{bmatrix} 0 \\ \sqrt{I_x^2 + I_y^2} \end{bmatrix} \end{aligned} \tag{20}$$

The interpretation of this result is rather simple. The gradient magnitude is the directional derivative parallel to the direction of the gradient. It is also invariant to rotations since the gradient response at any pixel transforms to exactly the above defined vector (20). The second derivative may similarly be expressed. There are several ways in which one may construct the rotation matrix $\boldsymbol{R}$. Further, given a multiscale derivative feature vector to any order, an infinite number of rotational invariants may be constructed.

However, Florack (8) has shown that given the derivatives of an image I up to a certain order, only a finite number of *irreducible differential invariants* exist, and they may be computed in a systematic manner. The irreducible set of invariants up to order two of an image I are

$$\begin{aligned} d_0 &= I && \text{(intensity)} \\ d_1 &= I_x^2 + I_y^2 && \text{(magnitude)} \\ d_2 &= I_{zz} + I_{yy} && \text{(Laplacian)} \\ d_3 &= I_{xx}I_xI_x + 2I_{xy}I_xI_y + I_{yy}I_yI_y \\ d_4 &= I_{xx}^2 + 2I_{xy}^2 + I_{yy}^2 \end{aligned}$$

The reason these are termed irreducible is that other invariants (up to that order) may be expressed as combinations of them. Thus, the multiscale derivative vectors may be transformed so that they are invariant to 2-D rotations in the image plane. In the retrieval by appearance application we use the vector (minus the intensity term) $\boldsymbol{\Delta}_\sigma = \langle d_1, \ldots d_4 \rangle_\sigma$, computed at three different scales. This representation to a higher order has also been used by Schmid and Mohr (18) for object recognition.

Implementation

Filtering may be carried out either in the spatial domain using convolution or in the frequency domain using composition. In the latter case the Fourier transform and the inverse Fourier transform will need to be computed before and after the composition operation.

The choice of the domain for filtering is dependent on the size of the kernel. For an image of size N and filter of size w, the complexity of spatial domain filtering using separable filters is $O(wN)$, while that using frequency domain filtering is $O(N \log N + N^2/\omega^2)$. Thus, when the image and kernel sizes are small, spatial-domain filtering may be preferred, while for large images frequency-domain filtering may be advantageous. In addition, if several operations need to be performed, such as filtering with multiple derivatives, then frequency-domain filtering may be preferred.

In either domain, the issue of *discretization* has to be faced. The derivation in the previous section relied on continuous functions, whereas practical implementations require discrete versions of these filters. In addition, in the spatial domain, *truncation* effects need to be considered as well—that is, the effects of truncating the Gaussian to a finite extent. In this subsection the effects of discretizing and truncating the filter in the spatial domain will be discussed.

Discretizing Gaussians and Gaussian Derivatives. The derivations of the algorithms in the previous sections have assumed that the Gaussians and Gaussian derivatives were continuous functions. To apply them, they first need to be discretized. The discretization needs to be performed carefully, since errors can arise from it (6,19). A number of different procedures have been suggested in the literature. These include:

1. *Block Averaging.* The continuous kernel is averaged over each pixel, that is, the filter value is integrated over each pixel and then sampled (19). Let the discrete filter be defined over the values $-w$ to w (that is, its width is $2w + 1$). Then the value of the discrete Gaussian kernel at a point i is given by

$$g[i] = \int_{i-1/2}^{i+1/2} G(x, \sigma)\, dx = \operatorname{erf}\left(\frac{i + 1/2}{\sigma}\right) - \operatorname{erf}\left(\frac{i - 1/2}{\sigma}\right) \tag{21}$$

where er f$(x) = \int_0^x \exp(-t^2/2)\, dt$ is the error function. The first derivatives may be computed similarly. For example, the first derivative of the Gaussian in the x direction is given by

$$g_x[i] = \int_{i-1/2}^{i+1/2} G_x(x,\sigma)\, dx = G(i+1/2,\sigma) - G(1-1/2,\sigma) \tag{22}$$

2. *Discrete Derivative.* The Gaussian is first sampled. The image is then convolved with the sampled Gaussian, and the output convolved with a discrete version of the derivative. This approach is widely used. The discrete Gaussian kernel at a point i is given by

$$g[i] = G(i,\sigma) \tag{23}$$

A discrete version of the first derivative is given by the kernel $D = [-1, 0, 1]$. Then, a discrete version of the first Gaussian derivative in the x direction is given by

$$g_x = D * g[i] \tag{24}$$

Since convolution is associative, the image may first be filtered with the discrete Gaussian and the result may then be filtered with the first derivative kernel D. Second derivatives may be computed using the second-derivative kernel $D_2 = [-1, 2, -1]$.

3. *Sampled Gaussian Derivatives.* The continuous version of the Gaussian or Gaussian derivative is sampled directly at each pixel, and the sample values used for the discrete version of the filter. The sampled Gaussian derivative is given by

$$g_{x^n}[i] = G_{x^n}(i,\sigma) \tag{25}$$

4. *Discrete Scale Space.* The values of the discrete Gaussian are computed using a discrete scale space. The image is filtered with the discrete Gaussian and then filtered with a discrete version of the derivative. See Ref. 6 for how to compute the discrete Gaussian.

The question arises as to which technique is appropriate. It may be argued that block averaging takes account of the imaging process and may therefore be assumed to be the best discretization (19,6). For example, when a scene is imaged by a charge coupled device (CCD) camera, the output of each pixel is proportional to the total light falling over the entire area of each pixel (that is, the integral of the brightness over that pixel). The area is actually better approximated as a weighted integral—the weight being a Gaussian (6).

The results obtained using sampled Gaussian derivatives approximate those due to block averaging provided the scales (σ) used are large. As the scale is reduced, the errors due to using a sampled Gaussian derivative increase. Typically, below $\sigma = 0.5$ sampled Gaussian derivatives should not be used. In practice, most scales used are larger and hence sampling Gaussian derivatives are usually a good method of computing discrete Gaussian derivatives.

Assume that a large number of Gaussian derivatives need to be computed. Then for each order of a Gaussian derivative, the Gaussian needs to be sampled and the image filtered with the appropriate discrete kernel. This can be expensive. Consider, for example, the 1-D case, and assume that the image needs to be filtered with derivatives up to order 2. Let the kernel width for the discrete versions of the Gaussian, first derivative, and second derivative be $2w + 1$. Then to filter the image with Gaussian derivatives up to order 2 requires time proportional to $3(2w + 1) = 6w + 3$. This time may be reduced by using discrete derivatives to compute Gaussian derivatives. First, the image is filtered with a sampled Gaussian. The output of this image is filtered with the kernels D and $D2$, and this is equivalent to filtering the image with the first and second derivatives of the Gaussian. The time taken to filter, however, is only $2w + 7$. Since w may often be large, Gaussian derivative filtering accomplished using discrete derivatives is cheaper to compute than using sampled Gaussian derivatives. The tradeoff is that the results obtained using discrete derivatives are not as accurate. That is, sampled Gaussian derivatives are a better approximation to block averages than discrete Gaussian derivatives (see Ref. 20).

Truncation of Gaussian Derivatives. Gaussians and Gaussian derivatives are infinite in extent. However, most of their energies reside in a small region around the origin. Thus, for all practical purposes they may be truncated. Truncation also reduces the time taken to filter the images, since the resulting kernel sizes are smaller. There has been some discussion about where Gaussians and Laplacians of Gaussians should be truncated (21,19), but a general discussion of how Gaussian derivatives should be truncated seems to be absent in the literature (but see Ref. 20).

Figure 1 shows the truncation errors for different values of the truncation radius. The truncation error is computed as follows:

$$\text{truncation error} = \frac{\int_{-\infty}^{\infty} |G_{x^i}(x,\sigma)|\, dx - \int_{-k\sigma}^{k\sigma} |G_{x^i}(x,\sigma)|\, dx}{\int_{-\infty}^{\infty} |G_{x^i}(x,\sigma)|\, dx} \tag{26}$$

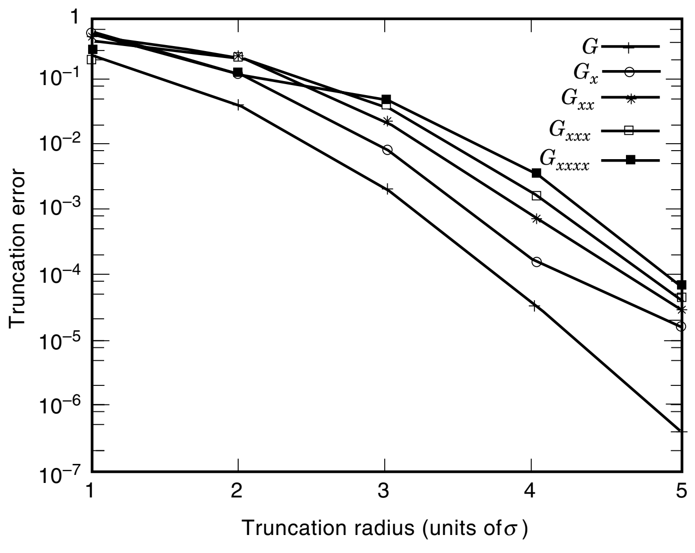

Figure 1. Truncation errors as a function of the truncation radius for Gaussians and Gaussian derivative filters. G denotes the Gaussian, and G_x, G_{xx}, G_{xxx}, and G_{xxxx} denote the first, second, third, and fourth Gaussian derivatives respectively. The truncation errors are taken as a proportion of the total integral of the absolute value of filter.

where $G_{x^i}(x, \sigma)$ is the ith-order Gaussian derivative (with G denoting the Gaussian) and k is the truncation radius. In the above equation, the difference between the integrals of the absolute values of the truncated function and the untruncated function is first computed. Then this difference is divided by the integral of the absolute values of the untruncated filter to give the truncation error as a proportion of the integral of the untruncated filter. Note that the truncation error is independent of σ. The truncation errors in Figure 1 were computed by summing over discrete versions of the filter using large σ's instead of computing the integrals analytically (the difference should be insignificant).

As Figure 1 shows, for a given truncation radius, the error increases with the order of the derivative. Many researchers assume that it suffices to truncate Gaussians so that the truncation radius is $\pm 2\sigma$, that is, the filter width is 4σ. For a truncation radius of 2σ, 96% of the energy of the Gaussian is contained within the filter width (i.e., the truncation error is 0.04). But for the same truncation radius, Gaussian derivatives have a much larger truncation error. For example, the first derivative of the Gaussian has an error of about 12% if it is truncated to within $\pm 2\sigma$, while higher derivatives have a much larger error. Figure 1 shows that the truncation error is less than 0.01 for the first four Gaussian derivatives if the truncation radius is greater than or equal to $\pm 4\sigma$. It may also be shown that the qualitative errors produced are large if the truncation radius is less than $\pm 4\sigma$ for derivatives up to order 4 (see Ref. (20).

Suggested Reading

Multiresolution representations are related to multiscale representations. A classical multiresolution representation, the Laplacian pyramid (2) may be generated as follows:

$$I^{(n)} = F[I^{(n-1)}]$$
$$I^{(0)} = Z_{xx} + Z_{yy}$$

where Z is the original image and $I^{(n)}$ is a representation at a coarser resolution. The operator F consists of two operations: the first one is a smoothing step, and the second is a subsampling step. The smoothing step is required to reduce aliasing effects due to subsampling and may be implemented using a Gaussian. A subsampling factor of 2 is typically used, so that a coarser image is a quarter the size of its immediate predecessor. Multiresolution representations may be used to compress images, detect features in a coarse-to-fine manner, and match features between images efficiently.

Multiresolution representations are related to, but somewhat different from, multiscale representations. Multiscale representations do not change the resolution of the original image, but rather vary the size of the operator. It is trivial to build a multiresolution representation from a multiscale representation, but the reverse is not true.

Although this section presents enough detail to motivate the use of Gaussian filtered representations, there are several aspects that are not covered. In particular, the study of scale space is abbreviated, and the user is referred to Refs. 11, 4, 6 for further review. Similarly, an in-depth study of rotational invariants is available in Ref. 8. For some additional properties of the Gaussian filter, such as optimality with respect to the uncertainty principle, the reader is referred to Ref. 22. In addition there is a physiological motivation for using Gaussian filtered representations. For example, Young (23) shows that visual receptive fields in the primate eye are better modeled by Gaussian derivatives.

Several researchers have used multiscale derivatives as a representation. In particular Ref. 14 uses multiscale vectors and the steerability property to recognize objects. In earlier work (15) derivatives were combined with the scaling theorems to retrieve visually similar objects at different sizes. The next section is also a good example of using multiscale derivatives. There they are used to recover the affine transform between deformed images.

MATCHING AFFINE DEFORMED IMAGES

In this section we will discuss how Gaussian and Gaussian-derivative filters may be used to match images under affine transforms. The ability to match two images or parts of images is required for many visual tasks. For example, recovering the structure of a scene requires matching two or more image patches arising from a scene viewed from different viewpoints. Other applications that require matching image patches include the registration of video sequences (24) and image mosaicking (25). Successive images of a scene when taken from different viewpoints are deformed with respect to each other. To first order, the transformation between images caused by viewpoint change may be modeled using an affine transform. The affine transform interprets the image motion in terms of an image translation and a deformation. In 2-D, the affine transformation may be described by the six parameters ($\boldsymbol{t}$, $\boldsymbol{A}$) where

$$r' = t + \boldsymbol{A}r \tag{27}$$

$\boldsymbol{r}'$ and $\boldsymbol{r}$ are the image coordinates related by an affine transform, $\boldsymbol{t}$ is a 2-by-1 vector representing the translation, and $\boldsymbol{A}$ the 2-by-2 affine deformation matrix. The affine transform is useful because the image projections of a small planar patch from different viewpoints are well approximated by it.

In general, affine transforms between image patches have been recovered in a number of different ways (for more details see Ref. 13):

1. Matching image intensities by searching through the space of all affine parameters. This approach adopts a brute force search strategy which is slow (26).
2. Linearizing the image intensities with respect to the affine parameters. This may be done at each pixel to give one equation per pixel. By assuming that the same affine transformation is valid over some region, an overconstrained system of equations is obtained. Linearization limits these algorithms to cases when the affine transforms are small (27–29).
3. Filtering the image with Gaussians and linearizing the filter outputs (30). The results are poor for general affine transforms because only the filter outputs from a single pixel are used.
4. Line-based methods that match the closed boundaries of corresponding regions (31,32). However, they are limited to homogeneous regions with closed boundaries.

5. Matching patches deformed under similarity transforms using the Mellin–Fourier transform (33). Although possible, recovery of the affine transform has not been demonstrated. The main drawback to these techniques is that they are inherently global and they are not applicable to general affine transforms.

The difficulty with measuring affine transforms is indicated in Fig. 2, where the image on the right is scaled to 1.4 times the image on the left. Even if the centroids of the two images are matched accurately, measuring the affine transform is difficult, since the sizes of every portion of the two images differ. This problem arises because traditional matching uses fixed correlation windows or filters. The correct way to approach this problem is to deform the correlation window or filter according to the image deformation.

Here, we present a computational scheme where Gaussian and derivative-of-Gaussian filters are used and the filters deformed according to the affine transformation. First, it is shown that if an image is filtered with a Gaussian (or Gaussian derivative), then the affine transformed version of the image needs to be filtered with a deformed Gaussian (or Gaussian derivative) if the two filter outputs are to be equal; the deformation is equal to the affine transform. Thus, the problem of recovering the affine transform may be recast into the problem of finding the deformation parameters of the Gaussian (or Gaussian derivative). For example let Z_1 and Z_2 be two images that differ by a scale change s. Then the output of Z_1 filtered with a Gaussian of σ will be equal to the output of Z_2 filtered with a Gaussian of $s\sigma$.

The resulting equations are solved by linearizing with respect to the affine parameters. Unlike the technique used in Ref. 30, the filter outputs from a number of points in a region are pooled together. This substantially improves the accuracy of the technique. For example, using Werkhoven and Koenderink's algorithm (30) on the images in Fig. 2 returns a scale factor of 1.16, while the algorithm here matches correctly and therefore returns a scale factor of 1.41.

Deformation of Filters

The initial discussion will assume zero image translation; translation can be recovered as suggested in the subsection "Finding the Image Translation" below. It is also assumed that shading and illumination effects may be ignored.

Consider two Riemann-integrable functions Z_1 and Z_2 related by an affine transform:

$$Z_2(\boldsymbol{Ar}) = Z_1(\boldsymbol{r}) \tag{28}$$

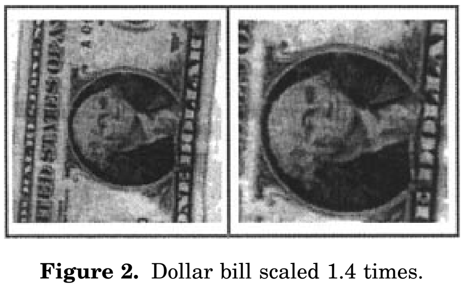

Figure 2. Dollar bill scaled 1.4 times.

Consider first the case where Z_1 is a scaled version of Z_2, that is,

$$Z_2(s\boldsymbol{r}) = Z_1(\boldsymbol{r}) \tag{29}$$

Then

$$\int Z_1(\boldsymbol{r})G(\boldsymbol{r},\sigma)\,d\boldsymbol{r} = \int Z_2(s\boldsymbol{r})G(\boldsymbol{r},\sigma)\,d\boldsymbol{r} \tag{30}$$

$$= \int Z_2(s\boldsymbol{r})G(s\boldsymbol{r},s\sigma)\,d(s\boldsymbol{r}) \tag{31}$$

That is, the output of Z_1 filtered with a Gaussian is equal to the output of Z_2 filtered with a scaled Gaussian. Note that this equation is also true for similarity transforms, that is, $\boldsymbol{A} = s\boldsymbol{R}$.

Define a generalized Gaussian by

$$G(\boldsymbol{r},\boldsymbol{M}) = \frac{1}{(2\pi)^{n/2}\det(\boldsymbol{M})^{1/2}}\exp\left(-\frac{\boldsymbol{r}^{\mathrm{T}}\boldsymbol{M}^{-1}\boldsymbol{r}}{2}\right) \tag{32}$$

where $\boldsymbol{M}$ is a symmetric positive semidefinite matrix. Then, if Z_1 and Z_2 are related by an affine deformation, the output of Z_1 filtered with a Gaussian is equal to the output of Z_2 filtered with a Gaussian deformed by the affine transform (see Refs. 20 and 34 for a derivation).

$$\int Z_1(\boldsymbol{r})G(\boldsymbol{r},\sigma^2\boldsymbol{I})\,d\boldsymbol{r} = \int Z_2(\boldsymbol{Ar})G(\boldsymbol{Ar},\boldsymbol{R\Sigma R}^{\mathrm{T}})\,d(\boldsymbol{Ar}) \tag{33}$$

where the integrals are taken from $-\infty$ to ∞. $\boldsymbol{R}$ is a rotation matrix and Σ a diagonal matrix with entries $(s_1\sigma)^2$, $(s_2\sigma)^2$, . . ., $(s_n\sigma)^2$, $(s_i \geq 0)$, and $\boldsymbol{R}\Sigma\boldsymbol{R}^{\mathrm{T}} = \sigma^2\boldsymbol{AA}^{\mathrm{T}}$ (this follows from the fact that $\boldsymbol{AA}^{\mathrm{T}}$ is a symmetric, positive semidefinite matrix).

Intuitively, Eq. (33) expresses the notion that the Gaussian-weighted-average brightnesses must be equal, provided the Gaussian is affine transformed in the same manner as the function. The problem of recovering the affine parameters has been reduced to finding the deformation of a known function, the Gaussian, rather than the unknown brightness functions.

The level contours of the generalized Gaussian are ellipses rather than circles. The tilt of the ellipse is given by the rotation matrix, while its eccentricity is given by the matrix Σ, which is actually a function of the scales along each dimension. The equation clearly shows that to recover affine transforms by filtering, one must deform the filter appropriately—a point ignored in previous work (26–28). The equation is local because the Gaussians rapidly decay.

The integral may be interpreted as the result of convolving the function with a Gaussian at the origin. It may also be interpreted as the result of a filtering operation with a Gaussian. To emphasize these similarities, it may be written as

$$Z_1 * G(\boldsymbol{r},\sigma^2\boldsymbol{I}) = Z_2 * G(\boldsymbol{r}_1,\boldsymbol{R\Sigma R}^{\mathrm{T}}) \tag{34}$$

where $\boldsymbol{r}_1 = \boldsymbol{Ar}$.

Similar equations may be written using derivative-of-Gaussian filters (for details see Refs. 20, 34).

Solution for the Case of Similarity Transforms

To solve Eq. (33) requires finding a Gaussian of the appropriate scale $s\sigma$ given σ. A brute force search through the space of scale changes is not desirable. Instead a more elegant solution is to linearize the Gaussians with respect to σ. This gives an equation linear in the unknown α:

$$\begin{aligned} Z_1 * G(\cdot, (\sigma)^2) &= Z_2 * G(\cdot, (s\sigma)^2) \\ &\approx Z_2 * G(\cdot, \sigma^2) + \alpha\sigma Z_2 * \frac{\partial G(\cdot, \sigma^2)}{\partial \sigma} \\ &= Z_2 * G(\cdot, \sigma^2) + \alpha\sigma^2 \nabla^2 Z_2 * G(\cdot, \sigma^2) \end{aligned} \tag{35}$$

where $s = 1 + \alpha$. The last equality follows from the diffusion equation $\partial G/\partial\sigma = \sigma\nabla^2 G$.

Equation (35) is not very stable if solved at a single scale. By using Gaussians of several different scales σ_i the following linear least-squares problem is obtained:

$$\sum_i \|Z_1 * G(\cdot, \sigma_i^2) - Z_2 * G(\cdot, \sigma_i^2) + \alpha\sigma_i^2 Z_2 * \nabla^2 G(\cdot, \sigma_i^2)\|^2 \tag{36}$$

It is solved using singular value decomposition (SVD).

It is not necessary to use every possible scale for σ_i. It turns out that the information at closely spaced scales is highly correlated and it usually suffices to use σ_i spaced apart by half an octave (a factor of about 1.4). For example, a possible set of scales would be (1.25, 1.7677, 2.5, 3.5355, 5.0).

Choosing a Different Operating Point

For large scale changes (say ≥ 1.2) the recovered scale tends to be poor. This is because the Taylor series approximation is good only for small values of α. The advantage of linearizing the Gaussian equations with respect to σ is that the linearization point can be shifted, that is, the right-hand side of Eq. (33) may be linearized with respect to a σ different from the one on the left-hand side to give the following equation:

$$Z_1 * G(\cdot, \sigma_i^2) \approx Z_2 * G(\cdot, \sigma_j^2) + \alpha' \sigma_j^2 Z_2 * \nabla^2 G(\cdot, \sigma_j^2) \tag{37}$$

where $s = \sigma_j/\sigma_i(1 + \alpha')$. The strategy therefore is to pick different values of σ_j and solve Eq. (37) (or actually an overconstrained version of it). Each of these σ_j will result in a value of α'. The correct value of α' is that which is most consistent with the equations. By choosing the σ_j appropriately, it can be ensured that no new convolutions are required.

In principle, arbitrary scale changes can be recovered using this technique. In practice, only a range of scales need to be recovered, and therefore a small set of operating points will suffice.

Finding the Image Translation

Image translation (optic flow) can be recovered in the following manner. Let Z_1 and Z_2 be similarity-transformed versions of each other (i.e., they differ by a scale change, a rotation, and a translation). Assume that an estimate of the translation $\boldsymbol{t}_0$ is available. Linearizing with respect to $\boldsymbol{r}$ and σ gives

$$\begin{aligned} Z_1(\boldsymbol{r} + t_0) * G(\boldsymbol{r}, \sigma^2) - \delta\boldsymbol{t}^{\mathrm{T}} Z_1(\boldsymbol{r} + \boldsymbol{t}_0) * G(\boldsymbol{r}, \sigma^2) \\ \approx Z_2 * G(\cdot, \sigma^2) + \alpha\sigma^2 Z_2 * \nabla^2 G(\cdot, \sigma^2) \end{aligned} \tag{38}$$

which is again linear in both the scale and the residual translation $\delta\boldsymbol{t}$. As before, an overconstrained version of this equation using multiple scales is obtained and solved for the unknown parameters. Large scales are handled as before.

$\boldsymbol{t}_0$ is obtained either by a local search or from a coarser level in a pyramid scheme, while $\delta\boldsymbol{t}$ is estimated from the equation.

Solving for the General Affine Transformation

There are two factors that need to be taken into account in the general case. First note that in the similarity case all the filtering was done at one point (the origin). The results may be further improved by filtering at many points rather than just one point. However, the rotation invariance will then be lost. In the general affine case, because of the larger number of parameters that have to be recovered, the filtering must be done at many points. The deformation must also be allowed for, and this can be done by linearizing the generalized Gaussian with respect to the affine parameters.

Filtering at a point $\boldsymbol{l}_i$ modifies the generalized Gaussian Eq. (33) as follows: Given a point with coordinates $\boldsymbol{l}_i$,

$$\int Z_1(\boldsymbol{r}) G(\boldsymbol{r} - \boldsymbol{l}_i, \sigma^2 \boldsymbol{I})\, d\boldsymbol{r} = \int Z_2(\boldsymbol{Ar}) G(\boldsymbol{A}(\boldsymbol{r} - \boldsymbol{l}_i)), \boldsymbol{R\Sigma R}^{\mathrm{T}})\, d(\boldsymbol{Ar}) \tag{39}$$

Thus if the image is filtered at point $\boldsymbol{l}_i$ in the first image patch, it must be filtered at point $\boldsymbol{Al}_i$ in the second image patch.

$$\begin{aligned} Z_1 * G(\boldsymbol{r} - \boldsymbol{l}_i, \sigma) \approx Z_2 * G(\boldsymbol{r}_1 - \boldsymbol{l}_i, \sigma) - \boldsymbol{Bl}_i)^{\mathrm{T}} Z_2 * G'(\boldsymbol{r}_1 - \boldsymbol{l}_i, \sigma) \\ + \sigma^2[b_{11} Z_2 * G_{xx}(\boldsymbol{r}_1 - \boldsymbol{l}_i, \sigma) \\ + b_{22} Z_2 * G_{yy}(\boldsymbol{r}_1 - \boldsymbol{l}_i, \sigma) \\ + (b_{12} + b_{21}) Z_2 * G_{xy}(\boldsymbol{r}_1 - \boldsymbol{l}_i, \sigma)] \end{aligned} \tag{40}$$

where the b_{ij} are elements of $\boldsymbol{B} = \boldsymbol{A} - \boldsymbol{I}$ and $\boldsymbol{I}$ is the identity matrix. Note that this is linear in the affine parameters b_{ij}. A number of methods incorporate the idea of filtering at many points (27–29). However, none of these compensate for the deformation terms (in essence, the difference between the traditional linearization methods and the technique presented here is the additional second-derivative terms).

Translation may be incorporated by noticing that the effect of translation is similar to that of $\boldsymbol{I}_i$. Thus, with translation included, the above equation may be rewritten as

$$\begin{aligned} Z_1 * G(\boldsymbol{r} - \boldsymbol{l}_i, \sigma) \approx Z_2 * G(\boldsymbol{r}_1 - \boldsymbol{l}_i, \sigma) - (\boldsymbol{Bl}_i)^{\mathrm{T}} Z_2 * G'(\boldsymbol{r}_1 - \boldsymbol{l}_i, \sigma) \\ + \sigma^2[b_{11} Z_2 * G_{xx}(\boldsymbol{r}_1 - \boldsymbol{l}_i, \sigma) \\ + b_{22} Z_2 * G_{yy}(\boldsymbol{r}_1 - \boldsymbol{l}_i, \sigma) \\ + (b_{12} + b_{21}) Z_2 * G_{xy}(\boldsymbol{r}_1 - \boldsymbol{l}_i, \sigma)] \\ - \boldsymbol{t}^{\mathrm{T}} Z_2 * G'(\boldsymbol{r}_1 - \boldsymbol{l}_i, \sigma) \end{aligned} \tag{41}$$

The equation may be turned into an overconstrained linear system by choosing a number of scales σ_i and a number of points $\boldsymbol{I}_i$. Two or three scales are chosen as before. The points $\boldsymbol{I}_i$ are picked as follows: either every point in the region is used, or a regularly spaced subset of the points are used. The resulting overconstrained system may be solved using least mean squares and minimizing with respect to the affine parameters. One way of writing the solution to this least-mean-squares system is

$$\boldsymbol{b} = \boldsymbol{M}^{-1}\boldsymbol{z} \tag{42}$$

where $\boldsymbol{b} = [a_{11} - 1, a_{12}, a_{21}, a_{22} - 1, t_x, t_y]$ are the required affine parameters, and the ith row of the n-by-6 matrix $\boldsymbol{M}$ is given by

$$[\sigma^2 Z_2 * G_{xx} - x_i Z_2 * G_x, \sigma^2 Z_2 * G_{xy} - y_i Z_2 * G_x$$
$$\sigma^2 Z_2 * G_{xy} - x_i Z_2 * G_y, \sigma^2 Z_2 * G_{yy} - y_i Z_2 * G_y, -Z_2 * G_x, -Z_2 * G_y] \quad (43)$$

where the Gaussian derivatives are taken at point $\boldsymbol{r}_1 - \boldsymbol{l}_i$. The ith element of the vector $\boldsymbol{z}$ is equal to $Z_1 * G(\boldsymbol{r} - \boldsymbol{l}_1, \sigma) - Z_2 * G(\boldsymbol{r}_1 - \boldsymbol{l}_1, \sigma)$.

The solution is done iteratively. At each step, the affine transformation is solved for. The image is then warped according to the transformation and the residual affine transformation solved for. The convergence is very rapid. A good solution is obtained using two scales 1.25, 1.77 spaced half an octave apart and with a window of size 13 by 13 (that is, points from a region of size 13 by 13 are selected) (20). The technique allows fairly large affine transforms to be recovered (scaling of as much as 40%).

The technique has some limitations. For large translations, a good initial estimate of the translation is required. This may be obtained in a number of ways. A coarse-to-fine technique may be used to estimate the translation. Alternatively, the method used to find similar points in the next section may be used to provide an estimate of the translation.

IMAGE RETRIEVAL

In this section Gaussian filtered representations of images are applied to the task of retrieval by image appearance. The paradigm used for retrieval is that a collection of images are represented using feature vectors constructed from Gaussian derivatives. During run time, a user presents an example image or parts thereof as a query to the system. The query's feature vectors are compared with those in the database, and the images in the database are ranked and displayed to the user.

There are several objectives that govern the design of a retrieval system. Primary among those are speed and the ability to find visually similar objects within a reasonable space of deformations. There is a third objective that can provide considerable flexibility to a user: the ability of a system to query parts of images if required. This is because a user may be interested in a part of an image such as a face in a crowd rather than a whole image such as a trademark. The interesting aspect of the algorithms presented here is that both these types of retrieval can be achieved without a system automatically trying to compute salient features or regions, which can be extremely challenging. All the system does in either case is compare signals (feature vectors). When the user has a notion of what is important in an image, it is exploited to find other vectors similar to it.

However, the desired flexibility imposes different constraints on the retrieval algorithms. Finding parts of images requires measurement of local similarity, and the representation must be local. Therefore, individual feature vectors might be used. On the other hand, finding whole images implies global similarity, and distributions of features can be used.

In previous work (15) derivative feature vectors in conjunction with the scaling theorems were used for retrieval by appearance. Database images were filtered with the Gaussian derivatives up to the second order, at several scales. A query image (or parts of it) was also filtered, but at a single scale. Then, using the scaling theorems given earlier in this article, the query feature vectors were correlated across scales with each database image's feature vectors. The results indicated that visually similar objects can be retrieved within about 25° of rotation. Similar results were shown by Rao and Ballard (14) in object recognition experiments.

However, correlation is slow. Further, it does not allow the feature vectors to be indexed. Thus, one cannot expect to develop a system of reasonable speed even for moderately sized databases using this method. Here, we present two progressively faster and indexable methods to retrieve images. The first method may be used to find parts of images, and the second for finding whole images. Finding parts of images requires similarities of local image features to be computed. This implies an explicit representation of local features. On the other hand, whole-image matching. In the next two sections the local and global similarity retrieval algorithms are elaborated.

Local-Similarity Retrieval

Local-similarity retrieval is carried out as follows. Database images are uniformly sampled. At each sampled location, the multiscale invariant feature vector $\boldsymbol{\Delta}_\sigma$ defined in the subsection "Rotational Invariants" above is computed at three different scales. Then, vectors computed for all the images in the database are indexed using a binary tree structure. During run time, the user picks an example image and designs a query. Since an image is described spatially (uniform sampling), parts of images or (imaged objects) can be selected. For example, consider Fig. 3(a). Here the user wants to retrieve white-wheeled cars and therefore selects the white wheel. The feature vectors that lie within this region are submitted to the system. Database images with feature vectors that match the set of query vectors both in feature space (L_2 norm of the vector) and coordinate space (matched image locations spatially consistent with query points) are returned as retrievals.

The approach for local-similarity retrieval is divided into two parts. During the off-line phase, images are sampled and multiscale derivatives are computed. These are transformed into rotational invariants and indexed. During the on-line phase, the user designs a query by selecting regions within an image. Feature vectors within the query are matched with those in the database, both in feature space and in coordinate space. The off-line and on-line phases are discussed next.

Off-Line Operations: Invariant Vectors and Indexing

Computing Features. A multiscale invariant vector is computed at sampled locations within the image. The vector, $\boldsymbol{\Delta}_\sigma = \langle d_1, \ldots d_4 \rangle_\sigma$ (see "Rotational Invariants" above), is computed at three different scales. The element d_0 is not used, since it is sensitive to gray-level shifts. The resulting multiscale invariant vector has at most twelve elements. Computationally, each image in the database is filtered with the first five partial derivatives of the Gaussian (i.e. to order 2) at three different scales at uniformly sampled locations. Then the multiscale invariant vector $\boldsymbol{D} = (\boldsymbol{\Delta}_{\sigma 1}, \boldsymbol{\Delta}_{\sigma 2}, \boldsymbol{\Delta}_{\sigma 3})$ is computed at those locations.

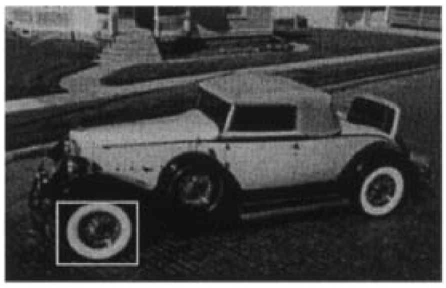

(a)

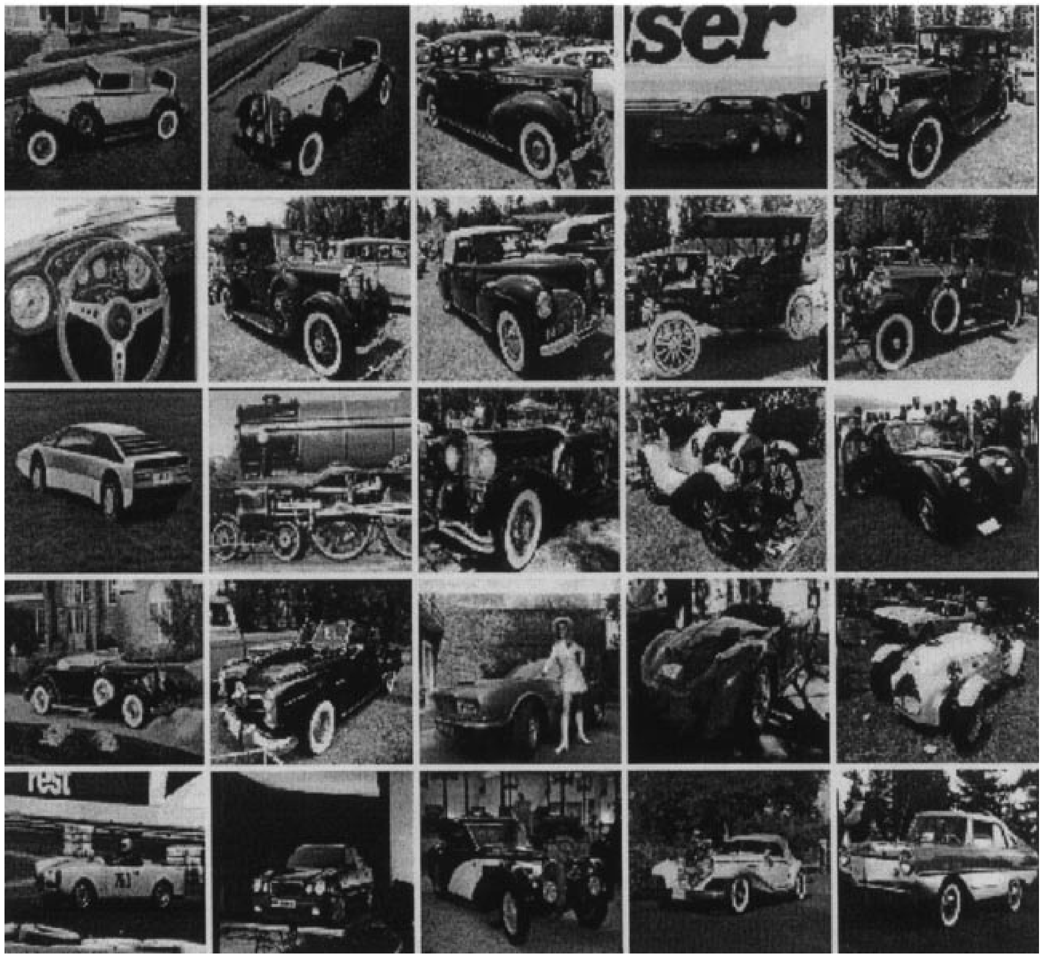

(b)

Figure 3. A query and its retrieval: (a) car query; (b) ranked retrieval.

Indexing. A location across the entire database may be identified by the *generalized coordinates,* defined as, $\boldsymbol{c} = (i, x, y)$, where i is the image number and (x, y) a coordinate within this image. The computation described above generates an association between generalized coordinates and invariant vectors. This association may be viewed as a table $M:(i, x, y, D)$ with $3 + k$ columns (k is the number of fields in an invariant vector) and a number of rows, R, equal to the total number of locations (across all images) where invariant vectors are computed. To retrieve images, a *find-by-value* functionality is needed, with which a query invariant vector is found within M and the corresponding generalized coordinate is returned. Inverted files (or tables) based on each field of the invariant vector are first generated for M. To index the database by fields of the invariant vector, the table M is split into k smaller tables $M'_1, \ldots, M'_k$, one for each of the k fields of the invariant vector. Each of the smaller tables M'_p, $p = 1, \ldots, k$, contains the four columns $[D(p), i, x, y]$. At this stage any given row across all the smaller tables contains the same generalized coordinate entries as in M. Then, each M'_p is sorted and a binary tree is used to represent the sorted keys. As a result, the entire database is indexed. A given invariant value can therefore be located in log R time (R = number of rows).

On-Line Operation. Run-time computation begins with the user selecting regions in an example image. At sampled locations within these regions, invariant vectors are computed and submitted as a query. The success of a retrieval in part depends on well-designed queries. More importantly, letting the user design queries eliminates the need for automatically detecting the salient portions of an object, and the retrieval may be customized so as to remove unwanted portions of the image. Based on the feedback provided by the results of a query, the user can quickly adapt and modify the query to improve performance.

The search for matching images is performed in two stages. In the first stage each query invariant is supplied to the find-by-value algorithm and a list of matching generalized coordinates is obtained. In the second stage a spatial check is performed on a per-image basis, so as to verify that the matched locations in an image are in spatial coherence with the corresponding query points. In this sub-subsection the find-by-value and spatial checking components are discussed.

Finding by Invariant Value. The multiscale invariant vectors at sampled locations within regions of a query image may be treated as a list. The nth element in this list contains the information $\boldsymbol{Q}_n = (\boldsymbol{D}_n, x_n, y_n)$, that is, the invariant vector and the corresponding coordinates. In order to find by invariant value, for any query entry $\boldsymbol{Q}_n$, the database must contain vectors that are within a threshold $\boldsymbol{t} = (t_1, \ldots, t_k) > 0$. The coordinates of these matching vectors are then returned. This may be represented as follows. Let $\boldsymbol{p}$ be any normalized invariant vector stored in the database. Then $\boldsymbol{p}$ matches the normalized query invariant entry $\boldsymbol{D}_n$ only if $\boldsymbol{D}_n - t < \boldsymbol{p} < \boldsymbol{D}_n + \boldsymbol{t}$. To implement the comparison operation two searches can be performed on each field. The first is a search for the lower bound, that is, the smallest entry larger than $D_n(j) - t(j)$, and the second is a search for the upper bound, that is the largest entry smaller than $D_n(j) + t(j)$. The block of entries between these two bounds are those that match the field j. In the inverted file, the generalized coordinates are stored along with the individual field values, and the block of matching generalized coordinates are copied from disk. Then an intersection of all the returned block of generalized coordinates is performed. The generalized coordinates common to all the k fields are the ones that match query entry $\boldsymbol{Q}_n$. The find-by-value routine is executed for each $\boldsymbol{Q}_n$, and as a result each query entry is associated with a list of generalized coordinates that it matches.

Spatial Fitting. The association between a query entry $\boldsymbol{Q}_n$ and the list of f generalized coordinates that match it by value may be written as

$$\begin{aligned}\boldsymbol{A}_n &= \langle x_n, y_n, c_{n1}, c_{n2}, \ldots, c_{nf}\rangle \\ &= \langle x_n, y_n, (i_{n1}, x_{n1}, y_{n2}), \ldots, (i_{nf}, x_{nf}, y_{nf})\rangle\end{aligned}$$

Here x_n, y_n are the coordinates of the query entry $\boldsymbol{Q}_n$ and c_{n1}, . . ., c_{nf} are the f matching generalized coordinates. The notation c_{nf} implies that the generalized coordinate c matches n and is the fth entry in the list. Once these associations are available, a spatial fit on a per-image basis can be performed. Any image u that contains two points (locations) that match some query entry m and n respectively are coherent with the query entries m and n only if the distance between these two points is the same as the distance between the query entries that they match. Using this as a basis, a binary fitness measure may be defined as

$$\mathscr{F}_{m,n}(u) = \begin{cases} 1 & \text{if} \quad \exists j \exists k : |\delta_{m,n} - \delta_{c_{mj}, c_{nk}}| \le T \\ & \qquad\qquad\qquad i_{m_j} = i_{n_k} = u,\ m \ne n \\ 0 & \text{otherwise} \end{cases}$$

where $\delta_{m,n}$ is the Euclidean distance between the query points m and n, and $\delta_{c_{mj}, c_{nk}}$ is the Euclidean distance between the generalized coordinates c_{mj} and c_{nk}. That is, if the distance between two matched points in an image is close to the distance between the query points that they are associated with, then these points are spatially coherent (with the query). Using this fitness measure, a match score for each image can be determined. This match score is simply the maximum number of points that together are spatially coherent (with the query). Define the match score by score(u) $\equiv \max_m \sum_{n=1}^{f} \mathscr{F}(u)_{m,n}$. The computation of score(u) is at worst quadratic in the total number of query points. The array of scores for all images is sorted, and the images are displayed in the order of their score. T used in $\mathscr{F}$ is a threshold and is typically 25% of $\delta_{m,n}$. Note that this measure not only will admit points that are rotated, but will also tolerate other deformations as permitted by the threshold. It is placed to reflect the rationale that similar images will have similar responses but not necessarily under a rigid deformation of the query points.

Experiments. The database used for the local similarity retrieval has digitized images of cars, steam locomotives, diesel locomotives, apes, faces, people embedded in different backgrounds, and a small number of other miscellaneous objects such as houses. 1561 images were obtained from the Internet and the Corel photograph—CD collection to construct this database. These photographs were taken with several different cameras of unknown parameters, and under varying uncontrolled lighting and viewing geometry.

Prior to describing the experiments, it is important to clarify what a correct retrieval means. A retrieval system is expected to answer queries such as "find all cars similar in view and shape to this car" or "find all faces similar in appearance to this one." In the examples presented here the following method of evaluation is applied. First, the objective of the query is stated, and then retrieval instances are gauged against the stated objective. In general, objectives of the form "extract images similar in appearance to the query" will be posed to the retrieval algorithm.

A measure of the performance of the retrieval engine may be obtained by examining the recall–precision table for several queries. Briefly, recall is the proportion of the relevant material actually retrieved, and precision is the proportion of retrieved material that is relevant (35). Consider as an example the query described in Fig. 3(a). Here the user wishes to retrieve white-wheeled cars similar to the one outlined and submits the query. The top 25 results, ranked in textbook fashion, are shown in Fig. 3(b). Note that although there are several valid matches as far as the algorithm is concerned (for example, image 12 is a train with a wheel), they are not considered valid retrievals as stated by the user and are not used in measuring the recall and precision. This yields an

Table 1. Queries Submitted to the System and Expected Retrieval

Given (User Input)	Find	Precision (%) 3 pixels	Precision (%) 5 pixels
Face	All faces	74.7	61.5
Face	Same person's face	61.7	75.5
Ape's coat [Fig. 6(a)]	Dark-textured apes [Fig. 6(b)]	57.5	57
Both wheels	White-wheeled cars	57.0	63.7
Coca-Cola logo	All Coca-Cola logos	49.3	74.9
Wheel [Fig. 3(a)]	White-wheeled cars [Fig. 3(b)]	48.6[a]	54.4
Patas monkey face	All vislble patas monkey faces	44.5	47.1

[a] See text.

inherently conservative estimate of the performance of the system. The average precision (over recall intervals of 10) is 48.6%. [The quantity n (= 10) is simply the number of retrievals up to recall n.]

One of the important parameters in constructing indices is the sample rate. Recall that indices are generated by computing multiscale invariant feature vectors at uniformly sampled locations within the image. The performance of the system is evaluated under sample rates of 3 pixels and 5 pixels. The case where every pixel is used could not be implemented due to prohibitive disk requirements and lack of resources to do so. Six other queries that were also submitted are depicted in Table 1. The recall–precision table over all seven queries is in Table 2. The second column of the table shows the average precision for each query with a database sampling of 5 pixels, while the third column displays the average precision for a sampling of 3 pixels. This compares well with text retrieval, where some of the best systems have an average precision of 50% (according to personal communication with Bruce Croft). The average precision over the same seven queries is 56.2% for the 5 pixel case and 61.7% for the 3 pixel case. However, while the increase in sampling improves the precision, it results in an increased storage requirement.

Unsatisfactory retrieval occurs for several reasons. First, it is possible that the query is poorly designed. In this case the user can design a new query and resubmit. A second source of error is in the matching itself. It is possible that locally the intensity surface may have very close values. Many of these false matches are eliminated in the spatial checking phase. Errors may also occur in the spatial checking phase because it admits much more than a rotational transformation of points with respect to the query configuration. Overall, the performance to date has been very satisfactory, and we believe that by experimentally evaluating each phase the system can be further improved. The time it takes to retrieve images depends linearly on the number of query points. On a Pentium Pro 200 MHz Linux machine, typical queries execute in between 1 and 6 min.

Table 2. Precision at Standard Recall Points for Seven Queries

Recall	Precision (%) 5 pixels	Precision (%) 3 pixels
0	100	100
10	95.8	100
20	90.3	90.4
30	80.1	80.9
40	67.3	75.7
50	48.9	55.9
60	39.9	49.4
70	34.2	47.6
80	31.1	40.6
90	18.2	20.7
100	12.4	17.1
Average	56.2	61.7

The primary limitations of the local matching technique are that it is relatively slow and that it requires considerable disk space. Further, as presented the system cannot search for images in their entirely. That is, it does not address global similarity.

Global-Similarity Retrieval

The same Gaussian derivative model may be used to efficiently retrieve by global similarity of appearance. Since the task is to find similarity of whole images, significant improvements in space as well as speed may be achieved by representing images using distributions of feature vectors as opposed to the vectors themselves. One of the simplest ways of representing a nonparametric distribution is a histogram. Thus, a histogram of features may be used.

There are several features that may be exploited. Here the task is to robustly characterize the 3-D intensity surface. A 3-D surface is uniquely determined if the local curvatures everywhere are known. Thus, it is appropriate that one of the features be local curvature. The principal curvatures of the intensity surface are differential invariants. Further, they are invariant to monotonic intensity variations, and their ratios are in principle insensitive to scale variations of the entire image. However, spatial orientation information is lost when constructing histograms of curvature (or ratios thereof) alone. Therefore we augment the local curvature with local phase, and the representation uses histograms of local curvature and phase.

Computing the Global Similarity. Three steps are involved in computing global similarity. First, local derivatives are computed at several scales. Second, derivative responses are combined to generate local features, namely, the principal curvatures and phases, and their histograms are generated. Third, the 1-D curvature and phase histograms generated at several scales are matched. These steps are described next.

Computing Local Derivatives. Derivatives are computed stably using the formulation shown in Eq. (3). The first and second derivatives are computed at several scales by filtering the database images with Gaussian derivatives.

Feature Histogram. The normal and tangential curvatures of a 3D surface (X, Y, intensity) are defined by (8)

$$N(\boldsymbol{p}, \sigma) = \frac{I_x^2 I_{yy} + I_y^2 I_{xx} - 2 I_x I_y I_{xy}}{(I_x^2 + I_y^2)^{3/2}} (\boldsymbol{p}, \sigma)$$

$$T(\boldsymbol{p}, \sigma) = \frac{(I_x^2 - I_y^2) I_{xy} + (I_{xx} - I_{yy}) I_x I_y}{(I_x^2 + I_y^2)^{3/2}} (\boldsymbol{p}, \sigma)$$

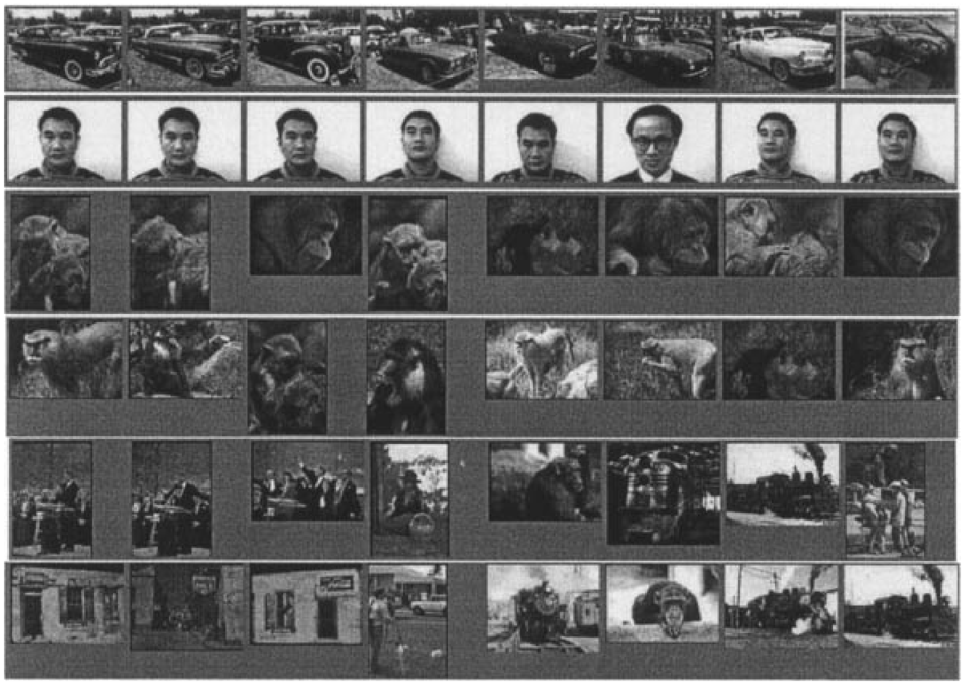

Figure 4. Image retrieval using curvature and phase.

where $I_x(\boldsymbol{p}, \sigma)$ and $I_y(\boldsymbol{p}, \sigma)$ are the local derivatives of the image I around point $\boldsymbol{p}$ using Gaussian derivatives at scale σ. Similarly, $I_{xx}(\cdot, \cdot)$, $I_{xy}(\cdot, \cdot)$, and $I_{yy}(\cdot, \cdot)$ are the corresponding second derivatives. The normal curvature N and tangential curvature T are then combined (36) to generate a shape index as follows:

$$C(\boldsymbol{p}, \sigma) = \arctan\left(\frac{N+T}{N-T}\right)(\boldsymbol{p}, \sigma)$$

The index value C is $\pi/2$ when $N = T$, and is undefined and therefore not computed when N and T are both zero. This is interesting because very flat portions of an image (or ones with constant ramp) are eliminated. For example in Fig. 4 (second row), the background in most of these face images does not contribute to the curvature histogram. The curvature index or shape index is rescaled and shifted to the range [0, 1], as is done in Ref. 37. A histogram is then computed of the valid index values over an entire image.

The second feature used is phase. The phase is simply defined as $P(\boldsymbol{p}, \sigma) = \arctan 2[I_y(\boldsymbol{p}, \sigma)/I_x(\boldsymbol{p}, \sigma)]$. Note that P is defined only at those locations where C is defined, and ignored elsewhere. As with the curvature index, P is rescaled and shifted to lie in the interval [0, 1].

Although the curvature and phase histograms are in principle insensitive to variations in scale, in early experiments we found that computing histograms at multiple scales dramatically improved the results. An explanation for this is that at different scales different local structures are observed, and therefore multiscale histograms are a more robust representation. Consequently, a feature vector is defined for an image I as the vector $\boldsymbol{V}_i = \langle H_c(\sigma_1), \ldots, H_c(\sigma_n), H_p(\sigma_1), \ldots, H_p(\sigma_n)\rangle$, where H_p and H_c are the curvature and phase histograms respectively. We found that using five scales gives good results, and the scales used were from 1 to 4 in steps of half an octave.

Matching Feature Histograms. Two feature vectors are compared using the normalized cross-covariance defined as

$$d_{ij} = \frac{\boldsymbol{V}_i^{(m)} \cdot \boldsymbol{V}_j^{(m)}}{\|V_i^{(m)}\| \, \|V_j^{(m)}\|}$$

where $\boldsymbol{V}_i^{(m)} = \boldsymbol{V}_i - \text{mean}(\boldsymbol{V}_i)$.

Retrieval is carried out as follows. A query image is selected, and the query histogram vector $\boldsymbol{V}_j$ is correlated with the database histogram vectors $\boldsymbol{V}_i$ using the above formula. Then the images are ranked by their correlation score and displayed to the user. In this implementation, and for evaluation purposes, the ranks are computed in advance, since every query image is also a database image.

Experiments. The curvature–phase method was tested using two databases. The first is a trademark database of 2048 images obtained from the US Patent and Trademark Office (PTO). The images obtained from the PTO are large and binary, and were converted to gray level and reduced for the experiments. The second database is the collection of 1561 assorted gray-level images used for the local-similarity case.

In the following experiments an image is selected and submitted as a query. The objective of this query is stated and the relevant images are decided in advance. Then the retrieval instances are gauged against the stated objective. In general, objectives of the form "extract images similar in appearance to the query" will be posed to the retrieval algorithm. The measure of the performance of the retrieval engine is obtained by examining the recall–precision table for several queries.

Queries were submitted to each of the collections (trademark and assorted image collection) separately for the purpose of computing recall and precision. The judgment of relevance is qualitative. For each query in both databases the

Table 3. Precision at Standard Recall Points for Six Queries

	Precision (%)	
Recall	Trademark	Assorted
0	100	100
10	93.2	92.7
20	93.2	90.0
30	85.2	88.3
40	76.3	87.0
50	74.5	86.8
60	59.5	83.8
70	45.5	65.9
80	27.2	21.3
90	9.0	12.0
100	9.0	1.4
Average	61.1	66.3

relevant images were decided in advance. These were restricted to 48. The top 48 ranks were then examined to check the proportion of retrieved images that were relevant. All images not retrieved within 48 were assigned a rank equal to the size of the database. That is, they are not considered retrieved. These ranks were used to interpolate and extrapolate the precision at all recall points. In the case of assorted images, relevance is easier to determine and more similar for different users. However, in the trademark case it may be quite difficult to determine relevance, and therefore the recall and precision may be subject to some error. The recall–precision results are summarized in Table 3, and both databases are individually discussed below.

Figure 5 shows the performance of the algorithm on the trademark images. Each strip depicts the top eight retrievals, given the leftmost image as the query. Most of the shapes have roughly the same structure as the query. Six queries were submitted for the purpose of computing recall and precision depicted in Table 3.

Experiments were also carried out with assorted gray-level images. Six queries submitted for recall and precision are shown in Fig. 4. The leftmost image in each row is the query and is also the first retrieved. The rest, from left to right, are seven retrievals depicted in rank order. Flat portions of the background are never considered, because the principal curvatures are very close to zero and therefore do not contribute to the final score. Thus, for example, the flat background in Fig. 4 (second row) is not used. Notice that visually similar images are retrieved even when there is some change in the background (first row). This is because the dominant object contributes most to the histograms. On using a single scale, poorer results are achieved and background affects the results more significantly.

The results of these and other examples are discussed below, with the average precision over all recall points depicted in parentheses:

1. *Find Similar Cars (65%).* Pictures of cars (Fig. 3) viewed from similar orientations appear in the top ranks because of the contribution of the phase histogram. This result also shows that some background variation can be tolerated. The eight retrieval, although a car, is a mismatch and is not considered a valid retrieval for the purpose of computing recall and precision.
2. *Find Same Face (87.4%) and Find Similar Faces.* In the face query (Fig. 4, second row) the objective is to find the same face. In experiments with a University of Bern face database of 300 faces with 10 relevant faces each, the average precision over all recall points for all 300 queries was 78%. It should be noted that the system presented here works well for faces with the same representation and parameters used for all the other databases. There is no specific "tuning" or learning involved to retrieve faces. The query "find similar faces" resulted in a 100% precision at 48 ranks because there are far more faces than 48. Therefore it was not used in the final precision computation.
3. *Find Dark-Textured Apes (64.2%).* The ape query (Fig. 6) results in several light-textured apes and country scenes with similar texture. Although these are not mismatches, they are not consistent with the intent of the query, which was to find dark-textured apes.
4. *Find Other Patas Monkeys (47.1%).* Here there are 16 Patas monkeys in all and 9 within a small view varia-

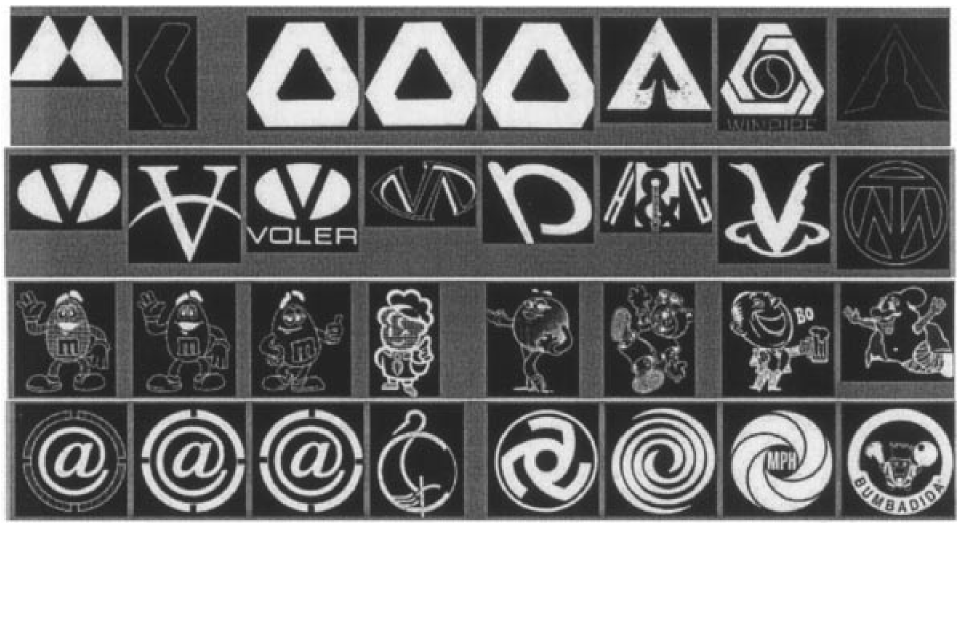

Figure 5. Trademark retrieval using curvature and phase.

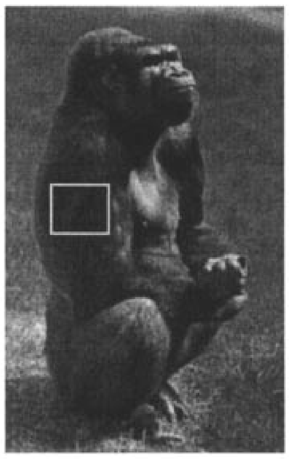
(a)

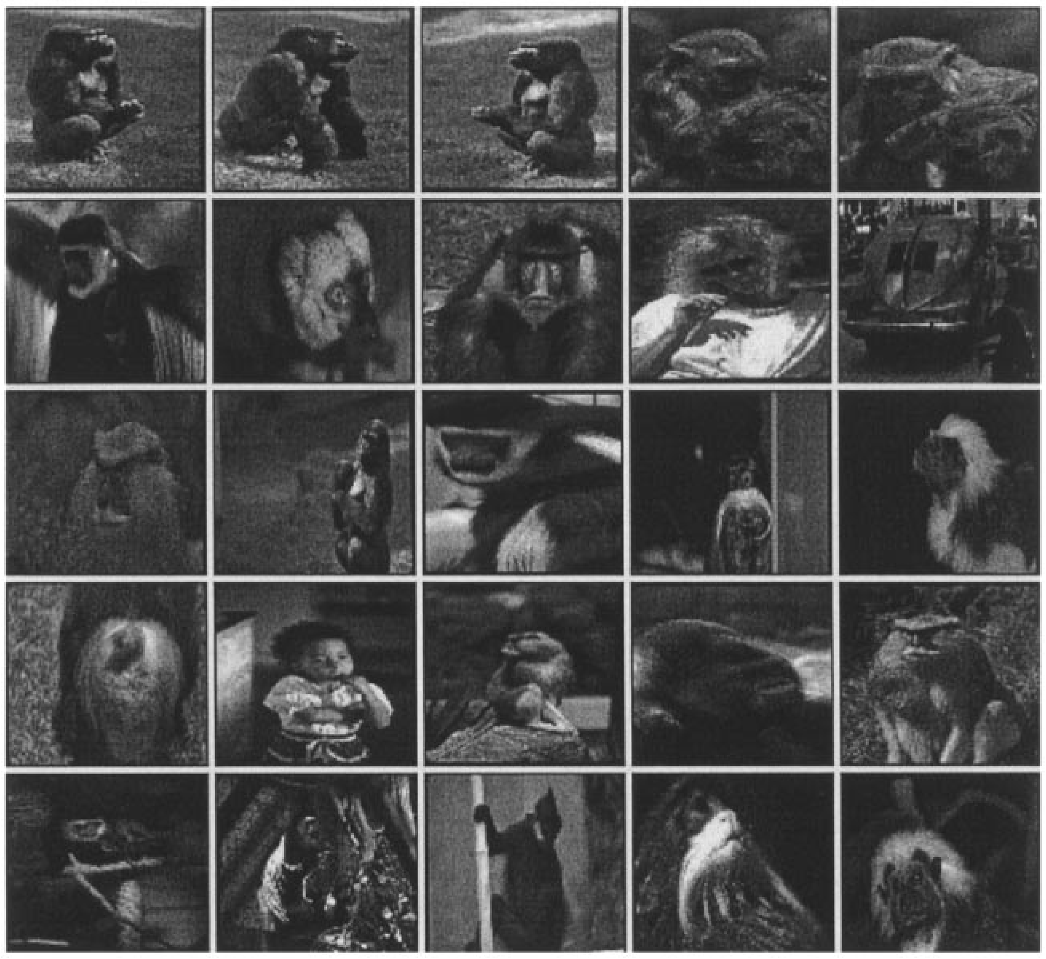
(b)

Figure 6. A query and its retrieval: (a) ape query; (b) ranked retrieval.

tion. However, here the whole image is being matched, so the number of relevant Patas monkeys is 16. The precision is low because the method cannot distinguish between light and dark textures, leading to irrelevant images. Note that it finds other apes (dark-textured ones), but those are deemed irrelevant with respect to the query.

5. *Given a Wall with a Coca-Cola Logo, Find Other Coca-Cola Images (63.8%).* This query (Fig. 4, last row) clearly depicts the limitation of global matching. Al-

though all three database images that had a certain texture of the wall (and also had Coca-Cola logos) were retrieved (100% precision), two other very dissimilar images with Coca-Cola logos were not.

6. *Scenes with Bill Clinton (72.8%).* The retrieval in this case (Fig. 4, fifth row) results in several mismatches. However, three of the four are retrieved in succession at the top, and the scenes appear visually similar.

While the queries presented here are not optimal with respect to the design constraints of global similarity retrieval, they are realistic queries that can be posed to the system. Mismatches can and do occur. The first is the case where the global appearance is very different. The Coca-Cola retrieval is a good example of this. Second, mismatches may occur at the algorithmic level. Histograms represent spatial information coarsely and therefore will admit images with nontrivial deformations. The recall and precision presented here compare well with text retrieval. The time per retrieval is of the order of milliseconds. In ongoing work we are experimenting with a database of 63,000 images, and the amount of time taken to retrieve is still less than a second. The space required is also a small fraction of the database. These are the primary advantages of global-similarity retrieval: to provide low-storage, high-speed retrieval with good recall and precision.

Suggested Reading

Image retrieval has attracted the attention of several researchers in recent years, and several retrieval systems have been proposed. The earliest general image retrieval systems were designed by Flickner et al. (38) and Pentland et al. (39). In Ref. 38 the shape queries require prior manual segmentation of the database, which is undesirable and not practical for most applications.

Several authors have tried to characterize the appearance of an object via a description of the intensity surface. In the context of object recognition (40) one represents the appearance of an object using a parametric eigenspace description. This space is constructed by treating the image as a fixed-length vector and then computing the principal components across the entire database. The images, therefore, have to be size- and intensity-normalized, segmented, and trained. Similarly, using principal component representations described in Ref. 41, face recognition is performed in Ref. 42. In Ref. 43 the traditional eigenrepresentation is augmented by using more discriminant features and is applied to image retrieval. The authors apply eigenrepresentation to retrieval of several classes of objects. The issue, however, is that these classes are manually determined and training must be performed on each. The approach presented in this article is different from all the above in that eigendecompositions are not used at all to characterize appearance. Further, the method presented uses no learning, does not depend on constant-size images, and deals with embedded backgrounds (local similarity) and heterogeneous collections of images using local representations of appearance.

The method presented in Ref. 18 is similar to the local-similarity algorithm. However, there are some differences. Schmid and Mohr's algorithm does not allow the user to select query regions and relies on corners as features. The algorithm used to spatially compare the query vectors with those of a database image (spatial consistency) is also different. The motivation behind the algorithm presented here is that algorithms such as feature detection or segmentation, which are used to determine salient parts of an image, cannot be determined *a priori* in a general retrieval system, because it is not possible to define in advance the needs of a user. Thus instead of establishing an *a priori* bias towards any feature, images are uniformly sampled. The selection of salient portions of an image is obtained in the form of the user-defined query. In addition we find that using the lowest two orders rather than three orders gives better results in locating similar features.

With regard to the global retrieval algorithm, Schiele and Crowley (44) used a technique based on histograms for recognizing objects in gray-level images. Their technique used the outputs of Gaussian derivatives as local features. Several feature combinations were evaluated. In each case, a multidimensional histogram of these local features is then computed. Two images are considered to be of the same object if they had similar histograms. The difference between our approach and the one presented by Schiele and Crowley is that here we use ID (as opposed to multidimensional) histograms and further use the principal curvatures (which they do not use) as the primary feature.

Texture-based image retrieval is also related to the appearance-based work presented in this article. Using Wold modeling, Liu and Picard (45) try to classify the entire Brodatz texture, and Gorkani and Pickard (46) attempt to classify scenes, such as city and country. Of particular interest is work by Ma and Manjunath (47), who use Gabor filters to retrieve similar-texture images, without user interaction to determine region saliency.

ACKNOWLEDGMENT

The authors wish to thank Bruce Croft and the Center for Intelligent Information Retrieval for continued support of this work. This work is made possible due to efforts by Adam Jenkins, David Hirvonen, and Yasmina Chitti.

This material is based on work supported in part by the National Science Foundation, Library of Congress, and Department of Commerce under cooperative agreement number EEC-9209623, in part by the United States Patent and Trademark Office and Defense Advanced Research Projects Agency/ITO under ARPA order number D468, issued by ESC/AXS contract number F19628-95-C-0235, in part by the National Science Foundation under grant number IRI-9619117, and in part by NSF Multimedia CDA-9502639. Any opinions, findings, and conclusions or recommendations expressed in this material are those of the author(s) and do not necessarily reflect those of the sponsors.

BIBLIOGRAPHY

1. D. Marr and E. Hildreth, Theory of edge detection, *Proc. R. Soc. London B,* **B207**: 1980.
2. P. Burt and T. Adelson, The laplacian pyramid as a compact image code, *IEEE Trans. Commun.,* **COM-31**: 532–540, 1983.

3. J. L. Crowley and A. C. Parker, A representation for shape based on peaks and ridges in the difference of low-pass transform, *IEEE Trans. Pattern Anal. Mach. Intell.,* **6**: 156–169, 1984.
4. J. J. Koenderink, The structure of images, *Biol. Cybern.,* **50**: 363–396, 1984.
5. J. J. Koenderink and A. J. van Doorn, Representation of local geometry in the visual system, *Biol. Cybern.,* **55**: 367–375, 1987.
6. T. Lindeberg, *Scale-Space Theory in Computer Vision,* Norwell, MA: Kluwer, 1994.
7. B. M. ter Har Romeny, *Geometry Driven Diffusion in Computer Vision,* Norwell, MA: Kluwer, 1994.
8. L. M. J. Florack, *The syntactic structure of scalar images,* Ph.D. Thesis, University of Utrecht, 1993.
9. S. Ravela and R. Manmatha, Retrieving images by appearance, *IEEE Int. Conf. Comput. Vision,* 1998.
10. S. Haykin, *Communication Systems,* New York: Wiley, 1978.
11. A. P. Witkin, Scale-space filtering, *Proc. Int. Joint Conf. Artificial Intell.,* 1983, pp. 1019–1023.
12. R. Manmatha, Measuring the affine transform—I: Scale and rotation. *Proc. Comput. Vision Pattern Recognition Conf.,* 1993, pp. 754–755.
13. R. Manmatha and J. Oliensis, Measuring affine transform—I, scale and rotation, *Proc. DARPA Image Understanding Workshop,* Washington, 1993, pp. 449–458.
14. R. Rao and D. Ballard, Object indexing using an iconic sparse distributed memory, *Proc. Int. Conf. Comput. Vision,* 1995, pp. 24–31.
15. S. Ravela, R. Manmatha, and E. M. Riseman, Image retrieval using scale-space matching, *Computer Vision—ECCV '96, 4th Eur. Conf. Comput. Vision,* Cambridge, UK: Springer-Verlag, 1996, pp. 273–282.
16. W. T. Freeman and E. H. Adelson, The design and use of steerable filters, *IEEE Trans. Pattern Anal. Mach. Intell.,* **13**: 891–906, 1991.
17. S. Ravela et al., Adaptive tracking and model registration across distinct aspects, *Int. Conf. Intell. Robots Syst.,* 1995, vol. 1, pp. 174–180.
18. C. Schmid and R. Mohr, Combining greyvalue invariants with local constraints for object recognition, *Proc. Comput. Vision Pattern Recognition Conf.,* 1996.
19. R. Hummel and D. Lowe, Computational considerations in convolution and feature extraction in images, in J. C. Simon (ed.), *From Pixels to Features,* Amsterdam, The Netherlands: Elsevier, 1989, pp. 91–102.
20. R. Manmatha, *Matching affine-distorted images,* Ph.D. Thesis, Univ. Massachusetts, Amherst, 1997.
21. E. C. Hildreth, *The Measurement of Visual Motion,* Cambridge, MA: MIT Press, 1984.
22. G. Granlund and H. Knutsson, *Signal Processing for Computer Vision,* Norwell, MA: Kluwer, 1995.
23. R. A. Young, The Gaussian derivative model for spatial vision: I. Retinal mechanisms, *Spatial Vision,* **2** (4): 273–293, 1987.
24. H. S. Sawhney, S. Ayer, and M. Gorkani, Model-based 2D and 3D dominant motion estimation for mosaicing and video representation, *Proc. 5th Int. Conf. Comput. Vision,* 1995, pp. 583–590.
25. M. Irani, P. Anandan, and S. Hsu, Mosaic based representations of video sequences and their applications, *Proc. 5th Int. Conf. Comput. Vision,* 1995, pp. 605–611.
26. D. G. Jones and J. Malik, A computational framework for determining stereo correspondence from a set of linear spatial filters, *Proc. 2nd Eur. Conf. Comput. Vision,* 1992, pp. 395–410.
27. J. R. Bergen et al., Hierarchical model-based motion estimation, *Proc. 2nd Eur. Conf. Comput. Vision,* 1992, pp. 237–252.
28. M. Campani and A. Verri, Motion analysis from optical flow, *Comput. Vision Graph. Image Process. Image Understanding,* **56** (12): 90–107, 1992.
29. J. Shi and C. Tomasi, Good features to track, *Proc. Comput. Vision Pattern Recognition Conf.,* 1994, pp. 593–600.
30. P. Werkhoven and J. J. Koenderink, Extraction of motion parallax structure in the visual system I, *Biol. Cybern.,* 1990.
31. R. Cipolla and A. Blake, Surface orientation and time to contact from image divergence and deformation, *Proc. 2nd Eur. Conf. Comput. Vision,* 1992, pp. 187–202.
32. H. S. Sawhney and A. R. Hanson, Identification and 3D description of "shallow" environmental structure in a sequence of images, *Proc. Comput. Vision Pattern Recognition Conf.,* 1991, pp. 179–186.
33. J. Segman, J. Rubinstein, and Y. Y. Zeevi, The canonical coordinates method for pattern deformation: Theoretical and computational considerations, *IEEE Trans. Pattern Anal. Mach. Intell.,* **14**: 1171–1183, 1992.
34. R. Manmatha, A framework for recovering affine transforms using points, lines or image brightnesses, *Proc. Comput. Vision Pattern Recognition Conf.,* 1994, pp. 141–146.
35. C. J. van Rijsbergen, *Information Retrieval,* London: Butterworth, 1979.
36. J. J. Koenderink and A. J. Van Doorn, Surface shape and curvature scales, *Image and Vision Comput.,* **10** (8): 1992.
37. C. Dorai and A. Jain, Cosmos—a representation scheme for free form surfaces, *Proc. 5th Int. Conf. Comput. Vision,* 1995, pp. 1024–1029.
38. M. Flickner et al., Query by image and video content: The qbic system, *IEEE Comput. Mag.,* **28** (9): 23–30, 1995.
39. A. Pentland, R. W. Picard, and S. Sclaroff, Photobook: Tools for content-based manipulation of databases, *Proc. Storage Retrieval Image and Video Databases II,* SPIE, 1994, vol. 2, pp. 34–47.
40. S. K. Nayar, H. Murase, and S. A. Nene, Parametric appearance representation, in *Early Visual Learning,* London: Oxford Univ. Press, 1996.
41. M. Kirby and L. Sirovich, Application of the Karhunen–Loeve procedure for the characterization of human faces, *IEEE Trans. Pattern Anal. Mach. Intell.,* **12**: 103–108, 1990.
42. M. Turk and A. Pentland, Eigenfaces for recognition. *J. Cognitive Neurosci.,* **3**: 71–86, 1991.
43. D. L. Swets and J. Weng, Using discriminant eigenfeatures for retrieval, *IEEE Trans. Pattern Anal. Mach. Intell.,* **18**: 831–836, 1996.
44. B. Schiele and J. L. Crowley, Object recognition using multidimensional receptive field histograms, in B. Buxton and R. Cipolla (eds.), *Computer Vision—ECCV '96,* Lecture Notes in Computer Science 1, Cambridge, UK, *Proc. 4th European Conf. Comput. Vision,* New York: Springer-Verlag, 1996.
45. F. Liu and R. W. Picard, Periodicity, directionality, and randomness: Wold features for image modeling and retrieval, *IEEE Trans. Pattern Anal. Mach. Intell.,* **18**: 722–733, 1996.
46. M. M. Gorkani and R. W. Picard, Texture orientation for sorting photos "at a glance," *Proc. 12th Int. Conf. Pattern Recognition,* Oct. 1994, pp. A459–A464.
47. W. Y. Ma and B. S. Manjunath, Texture-based pattern retrieval from image databases, *Multimedia Tools Appl.,* **2** (1): 35–51, 1996.

S. Ravela
R. Manmatha
University of Massachusetts

GAUSSIAN WHITE NOISE. See KALMAN FILTERS AND OBSERVERS.

GENERALIZATION. See ARTIFICIAL INTELLIGENCE, GENERALIZATION.

GENERATING SET. See DIESEL-ELECTRIC POWER STATIONS.

GENERATION OF NOISE. See NOISE GENERATORS.

GENERATOR (OSCILLATOR), PUMP. See MICROWAVE PARAMETRIC AMPLIFIERS.

GENERATOR, RAMP. See RAMP GENERATOR.

GENERATORS, AC. See TURBOGENERATORS.

GENERATORS, DC. See DC MACHINES.

GENERATORS, DIESEL-ELECTRIC. See DIESEL-ELECTRIC GENERATORS.

GENERATORS, TURBINE. See TURBOGENERATORS.